NEW SIZING METHODOLOGY FOR COST MINIMIZATION OF GROUND COUPLED HEAT PUMP SYSTEMS CONSIDERING GROUNDWATER FLOW

Mémoire

Martin Samson

Maîtrise en génie mécanique

Maître ès sciences (M. Sc.)

Québec, Canada

RÉSUMÉ

Ce mémoire de maîtrise introduit une nouvelle méthodologie de conception et d'optimisation techno-économique de systèmes géothermiques qui tient compte des écoulements souterrains. Une revue de littérature est complétée et la problématique est définie en s'appuyant sur les manques à combler au niveau des procédures de dimensionnement actuelles. La nouvelle procédure de dimensionnement inclut, entre autre, les données hydrogéologiques, les charges thermiques du bâtiment et les coûts du système géothermique. De plus, elle améliore les méthodologies actuelles en incluant une approche analytique pour la modélisation des écoulements souterrains lors de la simulation du champ de puits géothermiques.

La méthodologie de recherche est présentée, y compris la stratégie d'optimisation, les fonctions G utilisées lors de la simulation énergétique et les défis rencontrés au cours de cette maîtrise. Les fonctions G sont calculées avec deux modèles analytiques: source cylindrique infinie et source linéique finie mobile. Une nouvelle simplification mathématique pour l'intégration des fonctions G dans la routine d'optimisation est démontrée, ce qui permet de réduire considérablement le temps de calcul (jusqu'à 25%), en plus de constituer un nouvel ajout aux méthodologies actuelles utilisant des fonctions G. Les procédures de test et l'analyse de la convergence sont également discutées.

La nouvelle méthode de dimensionnement comprend le calcul des coûts initiaux et opérationnels. Des variables de conception optimales (profondeur de forage, distance entre les trous de forage consécutifs, etc.) et des aménagements de champ de puits (nombre de puits dans la direction x) sont présentés pour différentes valeurs de conductivité thermique du sol et de vitesse d'écoulement des eaux souterraines. En outre, une étude paramétrique est réalisée pour mesurer l'impact de l'écoulement des eaux souterraines par rapport au champ de puits sur l'aspect économique du projet. Une comparaison simultanée des coûts initiaux et opérationnels est également effectuée, ce qui permet de fournir des notions intéressantes pour les processus de conception à critères multiples. Enfin, les conceptions optimisées sont testées en dehors des conditions d'opération nominales.

ABSTRACT

This master's thesis introduces a new sizing methodology for ground coupled heat pump (GCHP) systems which takes into account groundwater flow in order to achieve a techno-economic optimization of the total cost of the project. A literature review is presented and the problem is defined in order to show missing elements from current GCHP sizing procedures. The new sizing procedure includes hydrogeological data, building thermal loads, and GCHP system costs, while improving actual design methodologies by including an analytical approach for groundwater flow in the heat transfer simulation of the borefield.

The research methodology is presented, including the optimization strategy, the G-functions used during energy simulations, and the challenges encountered during this master's degree. The G-functions are calculated with two analytical models: infinite cylinder source (ICS) and moving finite line source (MFLS). A new mathematical simplification for the integration of G-functions in the optimization routine is derived, which considerably reduces computational time (by up to 25%) and is a new addition to current methodologies using G-functions. Testing procedures and a convergence analysis are also discussed.

The new sizing methodology includes the calculation of the initial and the annual operational costs. Optimal design variables (borehole depths, distance between consecutive boreholes, etc.) and borefield layouts (number of boreholes in the x-direction) are presented for different values of ground thermal conductivity and groundwater velocity. In addition, a parametric study is done to measure the impact of the groundwater flow velocity and angle with respect to the borefield on the economics of the project. A simultaneous comparison of the initial and operational costs is also completed, as it can provide interesting insights for multi-criterion design processes. Finally, optimized designs are tested under off-design operating conditions.

CONTENTS

TABLE CAPTIONS

FIGURE CAPTIONS

NOMENCLATURE

Some variables listed in this section may have various meanings, depending on the chapter considered. This choice was made in order to use symbols that are consistent with those found in literature.

A	borefield aspect ratio (longest side/shortest side), [-]
B	distance between consecutive boreholes, [m]
c	specific heat, [J kg^{-1} K^{-1}]
C	cost, [$]
COP	coefficient of performance, [-]
f	fraction of maximum load, [%]
f	objective function, [-]
Fo	Fourier number $\alpha_g t / r_b^2$, [-]
G	G-function, [-]
G_N	overall G-function for N boreholes, [-]
G_1	G-function for a single borehole, [-]
G_{N1}	G-function due to borehole interaction, [-]
H	borehole depth, [m]
j	interest rate, [%]
k	thermal conductivity, [W m^{-1} K^{-1}]
L	length, [m]
$\dot{m}$	mass flow rate, [kg s^{-1}]
n	duration of the project, [years]
N	number of boreholes, [-]
$\Delta P'$	pipe head loss per unit length, [Pa m^{-1}]
Pe	Péclet number $u_g r_b / \alpha_g$, [-]
q	thermal load, [W]
r	radius, [m]

R	thermal resistance, [K W^{-1}]
t	time, [s]
T	temperature, [°C]
u	groundwater flow velocity, [m s^{-1}]
V_k	variable combination, [-]
w	work energy, [kWh]
$\dot{w}$	work or power, [W]
x	step size, [-]
X	price, [$]
Y_{1-7}	correlation coefficients, [-]
Z_{1-4}	correlation coefficients, [-]

Greek Symbols

α	thermal diffusivity, [m^2 s^{-1}]
β	correlation parameter, [-]
γ	correlation parameter, [-]
θ	average temperature change, [°C]
λ	under relaxation factor, [-]
μ	correlation parameter, [-]
ρ	density, [kg m^{-3}]
ϕ	groundwater flow angle, [°]
ω_k	correlation weight, [-]

Subscripts

a	annual
b	borehole
build	building
corr	correlation
drill	drilling
ex	excavation

$E1, 2$	electricity rates
f	fluid
g	ground
GHX	ground heat exchanger
HP	heat pump
ini	initial
op	operational
$pipe$	piping
P	power peak rate
ss	steady-state
tot	total
x, y	Cartesian directions

Acronyms

GCHP	ground coupled heat pump
ICS	infinite cylinder source
MFLS	moving finite line source
MILS	moving infinite line source
PAC	pompe à chaleur

REMERCIEMENTS

Ce mémoire de maîtrise a été réalisée grâce au soutien financier des organismes subventionnaires suivants : le Conseil de recherches en sciences naturelles et en génie du Canada (CRSNG) et le Fonds de recherche du Québec – Nature et technologies (FRQNT).

Je tiens à remercier le professeur Louis Gosselin pour m'avoir donné l'opportunité de réaliser ce projet de maîtrise. Il est un modèle d'accomplissement, autant sur le plan personnel que sur le plan professionnel. Son soutien et ses conseils furent indispensables tout au long de ma maîtrise, et je m'inspirerai de sa rigueur et de son enthousiasme lors de mes futurs projets. Ce fut un plaisir de travailler au sein du Laboratoire de Transferts Thermiques et d'Énergétique et j'y ai fait de belles rencontres. Je veux notamment remercier Jonathan Dallaire pour son support, son aide et ses encouragements lors de mes dernières sessions. Son expérience durement acquise fut bénéfique pour la réussite de ce mémoire.

Finalement, j'aimerais remercier mes proches pour m'avoir encouragé tout au long de mes études universitaires. Mes parents, Hélène et Claude, m'ont transmis leur curiosité scientifique et leur passion de la nature, tout en étant un modèle de réussite conjugale. Ils m'ont toujours soutenu dans la poursuite de mes études, et ce depuis mon plus jeune âge. Enfin, je remercie ma future épouse, Laurie-Anne. Sa présence rassurante à mes côtés m'a toujours encouragé dans les périodes difficiles. Je vois cette maitrise comme un tremplin qui nous propulsera ensemble vers les plus hauts sommets de la vie.

AVANT-PROPOS

L'article formant le corps de ce mémoire (Chapitre 3) a été coécrit par l'auteur de la thèse, Martin Samson, son directeur de recherche, Louis Gosselin, et le professionnel de recherche Jonathan Dallaire. La programmation, les simulations numériques, le traitement des résultats, les recherches, l'écriture de ce mémoire et l'essentiel de l'article ont été effectués par Martin Samson. La collaboration de Louis Gosselin a été indispensable quant à la supervision des travaux de recherche, à l'analyse des résultats, à l'aide à la rédaction et à la correction de l'article. Par rapport à la version originale, des modifications de forme ont été apportées à l'article afin d'en faciliter la lecture et pour être conforme aux exigences de la Faculté des études supérieures et postdoctorales (FESP). La pagination, les numéros de tableaux et de figures, l'inclusion des figures dans le texte et la numérotation des références bibliographiques ont été adaptées suivant le corps du mémoire. L'article scientifique inséré dans ce mémoire a été publié :

> **Chapitre 3 :** M. Samson, J. Dallaire, and L. Gosselin, "Influence of groundwater flow on cost minimization of ground coupled heat pump systems," Geothermics, vol. 73, pp. 100–110, May 2018.

CHAPTER 1 INTRODUCTION

1.1. Problem definition

Energy consumption has become an increasing issue over the last decades, particularly in the domain of building heating and cooling. Many efficient and ecofriendly technologies to provide those thermal needs have been recently developed, since several alternatives to fossil fuels are available, such as wind power, hydroelectric power, or geothermal energy. Geothermal heating and cooling is a technology of choice for a large variety of buildings in cold climate regions such as Canada. A ground coupled heat pump (GCHP) system can operate under low temperature conditions and still be efficient in terms of thermal performance [1], thus providing energy savings while having low environmental impacts. In fact, a geothermal system requires very little maintenance once it is installed and can have a lifetime of 20 years or more, depending on the durability of its components [2]. Accessible low cost green energy in the province of Québec, Canada, also gives a good incentive to realize such a project.

However, the high investment needed for the installation of a GCHP system can significantly impede the deployment of geothermal technology. Thus, an efficient sizing methodology is needed to avoid undersized or oversized designs which can lead to a reduction of the energy savings or an increase in the initial cost. Uncertainties on the ground thermal properties can also be problematic for the operational efficiency of the system. Thermal and hydrogeological response tests thus provide useful insights on local ground thermal conductivity and groundwater flow properties for any design procedure. In current sizing methodologies, the ground is usually simplified and represented by a homogeneous medium in which conduction is the only heat transfer mechanism.

Current sizing procedures usually try to find the required total borehole length for specified heating and cooling loads. From a techno-economic point of view, it is possible to optimize the design variables in order to minimize the total cost of the project. Such an approach has the advantage of identifying the optimal fraction of the building thermal loads to be supplied by the GCHP rather than imposing this fraction, i.e., the GCHP system is adapted to the building loads rather than the opposite.

Groundwater is commonly found in many geological environments, and it can significantly influence heat transfer around boreholes [3]–[6]. Analytical models have been developed to consider the effect of groundwater flow on heat transfer around a borefield. Yet, there is currently no sizing methodologies for cost minimization of GCHP systems considering groundwater flow.

1.2. Literature review

Lord William Thomson Kelvin first introduced the concept of heat pumps in the 1850s [7]. Heat pumps work on the same principle as a refrigerator system: they absorb heat from a heat source and change the working fluid into a gaseous state, the pressure of which is increased in a compressor, and then release heat to a heat sink which returns the working fluid to liquid phase. For a GCHP heating application, the heat source is the ground itself and the heat sink is usually the building's indoor air. Such systems can also serve for cooling applications: the heat source and sink are simply reversed. Geothermal energy is considered a renewable energy, and its utilization has been growing over the last few decades. Recently, Staffell et al. (2012) [2] provided an exhaustive review of the current situation for domestic heat pumps. According to Lund and Boyd (2016) [8], geothermal heat pumps represented the largest installed capacity (70.90%) and energy use (55.15%) of the worldwide capacity and direct utilization of geothermal energy in 2015. This technology emits greenhouse gases at almost a zero rate, when the source of electricity is green [9]. Combined with the clean energy available in the province of Québec [10], GCHP systems are an interesting option for heating and cooling buildings, since they provide energy savings and have low environmental impacts compared to other systems [11], [12]. Vertical heat exchangers, or boreholes, are the most widely used configuration for closed-loop systems, although horizontal borefields or open loop systems are also possible for geothermal heat pumps [9].

The impact of groundwater flow on the thermal performances of a GCHP system has been extensively studied [3]–[6]. In 1987, Eskilson [13], who can be seen as a pioneer in the field of ground heat exchangers analysis, developed analytical equations for solving heat transfer

in the ground including groundwater advection. However, his analytical solutions were developed for a single borehole under steady-state conditions only, and it only gave the temperature at borehole mid-height, thus requiring a correction factor to obtain the average temperature on the borehole.

Since then, different attempts were made to investigate the effect of groundwater flow on heat transfer around boreholes. Development of analytical models considering groundwater flow was undertaken by Sutton et al. (2003) [14] and Diao et al. [15] (2004). The former developed a new ground thermal resistance that accounts for groundwater flow, while the latter obtained an analytical solution to the equation for transient and steady-state temperature behavior in the ground with groundwater flow. Their models were both based on the moving infinite line heat source (MILS) theory. In order to account for axial effects along the boreholes, the moving finite line source (MFLS) was developed by Molina-Giraldo et al. (2011) [16]. They showed that these effects are even more important for long simulation times and short borehole lengths.

Numerical models accounting for groundwater flow are also widely available in the literature [17]–[21]. For example, Angelotti et al. (2014) [17] presented a numerical model of a single U-pipe heat exchanger in a sandy aquifer and a rigorous validation of the model under a broad range of groundwater velocities was provided. Geng et al. (2016) [21] presented optimization strategies to mitigate thermal anomalies in downstream boreholes. A finite element numerical simulation supported their work.

An alternative procedure was presented by Tye-Gingras and Gosselin (2014) [22]. They introduced a methodology for computing time-dependent ground response functions (G-functions) of vertical ground exchangers in the presence of groundwater flow. Borehole-to-borehole thermal interactions are accounted for in multi-borehole fields, and the procedure can be used for a large range of design parameters, ground properties, and time scales. The solution approach combines two analytical models: infinite cylinder source (ICS) and moving finite line source.

In regards to design methodologies, the most widely used procedure for sizing a geothermal borefield is that proposed by Kavanaugh and Rafferty (1997) [23] in their handbook from the American Society of Heating, Refrigerating and Air-Conditioning Engineers (ASHRAE). Given the heating or cooling load assumed by the designer for the ground, the procedure estimates the required length of boreholes by combining three factors: the average annual load over 10 years, the average monthly load over 30 days, and the peak load for 6 hours. The designer also assumes a certain grid of boreholes and a penalty temperature is considered in order to account for borehole-to-borehole thermal interactions in that configuration. However, this procedure does not correctly account for groundwater flow.

Recent studies have proposed another approach to GCHP system sizing by identifying the design minimizing the total cost of the system, which includes initial cost and operational cost. Robert and Gosselin (2014) [24] presented a procedure that determines the optimal number of boreholes, their depth and spacing, and the optimal size of the heat pump with an iterative approach. An hourly simulation for the operational cost computation is done using the finite line source model (FLS). The methodology was tested for different ground thermal conductivity and heat demands. The economic benefits of a thermal response test were also studied. Overall, the method could be used in a variety of contexts and applications, and could easily be adapted to include many costs and constraints. Hénault et al. (2016) [25] presented a new strategy to optimize the net present value of a hybrid GCHP system. Their approach integrated six design and operation parameters, such as the project financial parameters, the hourly thermal load of the building, the control strategy, and the ground thermal properties. They used G-functions to simulate the heat transfer around the boreholes. The algorithm used to construct them came from Pasquier and Marcotte (2013) [26]. In both cases, optimizations have been realized within the software product MATLAB with the *fmincon* algorithm [27]. However, these methodologies did not include groundwater flow in their thermal analysis of the borefield.

One can see that the effects of groundwater flow on heat transfer around a borefield are well documented. Some recent approaches with analytical models allow a fast and accurate evaluation of these effects, which can be interesting from a design methodology point of

view. Advancements in sizing procedures for cost minimization of GCHP systems have been recently made. These procedures evaluate both the initial and operational costs of a project, and they attempt to minimize its total cost. However, there are currently no design methodologies that account for groundwater flow while minimizing the total cost of a GCHP project.

1.3. Objectives

The main objective of this work is to develop a new sizing methodology for cost minimization of ground coupled heat pump systems that takes into account groundwater flow. Specific objectives are defined as follow:

1. Develop a new design and optimization methodology that includes hydrogeological data, building thermal loads, and GCHP system costs.
2. Improve actual design methodologies by including an analytical approach for groundwater flow in the heat transfer simulation of the borefield.
3. Develop a better understanding of the influential factors on the economics of a GCHP project by realizing a parametric study of the design variables and parameters.
4. Establish guidelines for the design of GCHP systems and develop a convenient design tool.

The research methodology used to achieve the aforementioned objectives of this work will be presented in Chapter 2. Finally, the new sizing methodology will be explained in detail in Chapter 3.

CHAPTER 2 METHODOLOGY

In this chapter, the research methodology used during this master's degree is presented. The numerical model was implemented with the commercial software product MATLAB, which also provides useful optimization tools. The goal of this chapter is to familiarize the reader with the different methods used in Chapter 3. In Section 2.1, the development of the optimization strategy used in Section 3.4 is discussed. The G-functions used in Section 3.3 to calculate the effect of groundwater flow on a geothermal borefield are presented in Section 2.2. Finally, the testing procedure used to validate the results of the sizing methodology (see Section 3.5) is discussed in Section 2.3.

2.1. Optimization strategy

Several different solvers can be used in MATLAB to find the optimal solution for a given problem [27]. In the current methodology, the total cost of a GCHP system is the objective function to minimize, and the design variables are the depth of the boreholes (H), the distance between two adjacent boreholes (B), and the fraction of the maximum load assumed by the GCHP system (f). These variables will be discussed in detail in Chapter 3. These variables are strongly coupled, which makes the optimization problem highly nonlinear. The design space is thus fairly large and the presence of local minima can often lead to non-optimal solutions. In this section, the problem definition and solver selection are first presented. Then, constraints of the optimization problem, tolerances on some of the optimization parameters, and the strategy used to select starting points are discussed.

2.1.1. Problem definition and solver selection

In order to use an optimization solver in MATLAB, the problem must be defined by an objective function with one or more input variables and one output variable, i.e., the function to minimize. The input variables, also known as optimization variables, specify the design space of the problem. The latter can either be large and sparse (with variables covering wide ranges of values) or small and dense. Large design spaces often lead optimization routines to get trapped in local minima, i.e., points in the design space where the objective function is lower than the solution given by the other points near them, but which are not the global

minimum solution. If the slope of the objective function is too steep around a local minimum, the solver may not be able to recover from it, thus the need to tune the procedure properly. The objective function used in the sizing methodology includes three input variables, H, B, and f, and one output variable, C_{tot} (the project total cost [$]). In order to calculate the total cost, two different costs are evaluated: the initial cost and the operational cost of the system, which are described in detail in Section 3.2.

The initial cost includes the cost of installing the necessary equipment, i.e., the drilling and excavation of the boreholes, the piping system, and the heat pump. These equipment costs depend on the input variables H, B, and f, since they determine the size of the borefield and the thermal load assumed by the heat pump. To evaluate the operational cost, an energy simulation of the system must be performed, as described in Section 3.3. The three input variables also significantly influence this cost, leading to a highly nonlinear problem. For example, increasing the depth of the boreholes increases the cost of drilling and piping, but it also enhances the amount of heat that can be transferred by each borehole, thus leading to a reduction of the operational cost.

The nonlinear solver *fmincon* can find the minimum of a constrained nonlinear multivariable function, thus being a suitable solver for the given problem. It uses an iterative procedure where the objective function is evaluated a certain number of times while its input variables change in order to find the optimal solution. It offers many possibilities for customizing the optimization, such as adding constraints, lower and upper bounds for the design variables (including starting points) and many other options to help the user make the resolution process as finely tuned as it can be. For all these reasons, it was decided that the solver *fmincon* would be used in the current methodology.

Different algorithms are available within the *fmincon* function in MATLAB, some of which are large-scale algorithms. An optimization algorithm is said to be large scale when it uses linear algebra that does not need to store or operate on full matrices. This is automatically and internally done in MATLAB by storing sparse matrices, and by using sparse linear

algebra for computations whenever possible. Medium scale methods, on the other hand, internally create full matrices and use dense linear algebra. If a problem is sufficiently large, full matrices take up a significant amount of memory, and the dense linear algebra may require a long time to execute. More information on the various algorithms is available in MATLAB Help [27]. Since it is simple to use, provides interesting possibilities, and is a large-scale algorithm, the *'interior point'* method was selected for the current problem. The design space defined by the three optimization variables is indeed large and sparse, with multiple orders of magnitude and some dimensions larger than the others, as shown in Chapter 3.

2.1.2. Constrained optimization

The first constraint that is applied to the current problem is the boundaries of the design variables. In order to delimit the design space, the *fmincon* function allows the use of a lower bound and an upper bound, which can be used simultaneously or only one at a time. In the current methodology, optimization boundaries were chosen to reflect the normal use of GCHP systems and the range of validity of prices for the initial cost of the GCHP project, both discussed in Chapter 3. Such systems do not usually cover all the heating or cooling needs of a building in order to have a steady-state operation, since building loads fluctuate a lot over time. Longer boreholes or wider distances between adjacent boreholes would cost more, as higher prices should be used for the drilling or the excavation cost to reflect the reality of the industry.

The second constraint that is applied was suggested by Robert and Gosselin [24] at the end of Section 4 of their paper: for a given project, an acceptable range of maximum load per unit of total length for the entire borefield must be respected, i.e.,:

$$\dot{q}_{\min} \leq \frac{q_{heating,\max}}{NH} \leq \dot{q}_{\max} \tag{2.1}$$

where $\dot{q}_{\min}$ and $\dot{q}_{\max}$ are the minimum and maximum load per unit lengh, $q_{heating,\max}$ is the maximum heating load requested by the simulated building, and N is the total number of boreholes. In their paper, Robert and Gosselin used 30 W/m and 130 W/m for the minimum

and maximum loads per unit of length, respectively, although these values are somewhat arbitrary. In fact, this constraint is used to limit the number of possible boreholes in the project. In the initial methodology, this constraint was implemented in the optimization routine, using the values mentioned previously. It was later found that the constraint given be Eq. (2.1) was always respected during optimization. Also, the layout of the borefield in the current work was arbitrarily limited to a single row of boreholes, i.e., borefield layouts ranging from 1×1 to 1×9. This could represent a project with only a limited area of terrain available for digging boreholes. For these reasons, the constraint on the maximum load per unit of total length for the entire borefield was not used in the final methodology.

2.1.3. Tolerance analysis

In addition to constraints and choice of algorithm, one can modify the tolerances of the solver on the size of a step and on the change in the value of the objective function during a step. This is known commonly as *'TolX'* and *'TolFun'* in MATLAB, as shown in Figure 2.1.

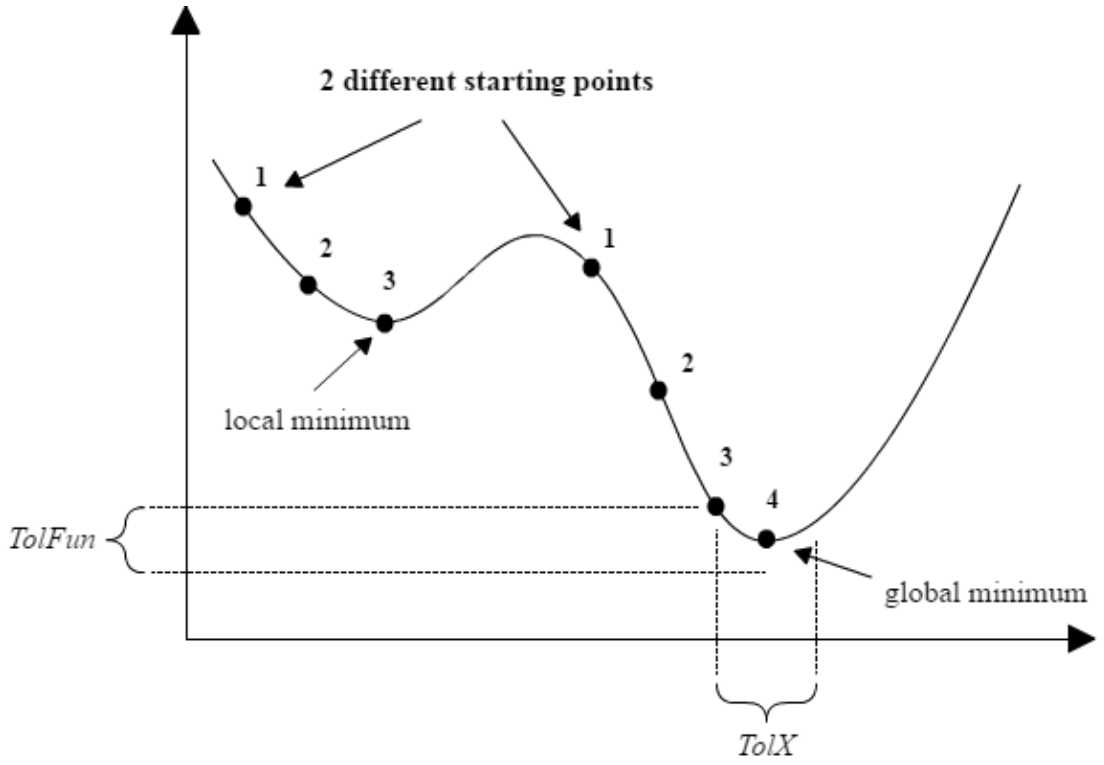

Figure 2.1: Tolerances and stopping criteria

If the solver attempts to take a step with a size $(x_i - x_{i+1})$ smaller than *'TolX'*, or if the objective function yields an output change $|f(x_i) - f(x_{i+1})|$ smaller than *'TolFun'* during a step, the iterative procedure ends. Different values for each tolerance have been tested to see their impact on the result of the objective function, and on the calculation time.

After investigation, the tolerance for the objective function was set to 10^{-2} and the tolerance on the size of the step was set to 10^{-3}. The total cost stops changing for smaller values, i.e., a smaller *TolX* or *TolFun* does not result in a more accurate prediction of the global minimum, but calculation time increases. For example, running a simulation with *TolX* = 10^{-4} and *TolFun* = 10^{-3} results in the same total cost as with the chosen values, but the calculation time was up to 120% longer depending on the starting points for the optimization.

2.1.4. Solver starting point problem

The last parameter used in this methodology with the solver *fmincon* was the starting point of the optimization routine. For each input variable, it is necessary to set a value from which the solver will start its first iteration. The different initial values for the three design variables must respect the boundaries previously discussed. During the development of the current methodology, validation tests were completed to see if the choice of the starting point (within the allowed design space) influenced the final optimal result. Because of the range for the boundaries of the design variables, the design space is quite large in two of the three directions, as seen in Table 3.2. H can vary from 45 to 105 m, B from 3 to 8 m, and f from 50 to 90%. The design space formed by these variables can be seen as a thin rectangular box in which the optimization could move to find the optimal combination of variables that yields a minimum project total cost. A clear conclusion was made during the investigation of the design space: due to its highly nonlinear nature, the objective function was subject to local minima. An example of a local minimum is shown in Figure 2.1. Unfortunately, these minima could prevent the solver from reaching the global minimum.

The first attempt to counter this behavior was to repeat the optimization routine for 4 different starting points, each determined randomly by a MATLAB subroutine. This solution provided a decent variability in the results while keeping the computation time in an acceptable range. Unfortunately, this methodology was not rigorous and stable enough to guarantee that the solver found the exact global minimum, since the randomness of the choice of the initial values did not guarantee a full coverage of the design space. Thus, it was decided to use 27 different starting points instead, i.e., 3 different starting values for each of H, B and f, set to the lower and upper boundaries, and a mid-range value. This way, the starting points covered the entire design space. This approach ensured that the global minimum of the project total cost for a given set of parameters was rigorously found during the optimization routine, even if the computational time was proportionally increased.

2.2. G-functions

In sizing methodologies of GCHP systems, the ground is usually simplified by assuming a homogeneous medium, with conduction being the only heat transfer mechanism. However, groundwater is mobile in many geological environments, and groundwater flow can significantly affect heat transfer around boreholes with the addition of heat advection. In his 1987 doctoral thesis, Eskilson [13] developed analytical equations to solve heat transfer equations in the ground including groundwater advection, but the solutions were developed for a single borehole in steady-state only. Since then, different attempts to investigate the effect of groundwater flow on heat transfer around boreholes have been made. The development of analytical models considering groundwater flow on the moving infinite line heat source (MILS) theory have been successful [14], [15]. The moving finite line source (MFLS) solution to account for axial effects was developed by [16]. Numerical models also exist to simulate accurately groundwater flow with high accuracy [5], but they require significantly more computational resources and time.

Ground functions (simply referred to as G-functions) are a convenient and simple way to assess the impact of groundwater flow. Tye-Gingras and Gosselin [22], for example, combined two analytical models, incorporating an infinite cylinder source (ICS) and a moving finite line source (MFLS), to create a comprehensive methodology for multi-borehole fields. Their G-functions allow an accurate prediction of heat transfer over a large range of design parameters, ground properties and time scales. One of the main challenges in the development of the new sizing methodology was to keep the computational time acceptable, which called for relying on G-functions rather than finite elements or other more expensive methods. In this section, a description of the G-function correlation developed by [22] will be presented. Then, some of the challenges encountered and the solutions found to facilitate the usage of G-functions will be presented, respectively.

2.2.1. Description of the G-function correlation

In their paper, Tye-Gingras and Gosselin [22] introduced a new mathematical model to enhance the computational efficiency of the G-functions with the MFLS model and the ICS model. Fortunately, existing MATLAB programs that compute these models were available, so that complete reprogramming was not to needed.

At this point, some definitions are necessary to the understanding of the methodology. G-functions presented here are based on a series of parameters, with some of them being dimensionless numbers: the Fourier number (Fo) and the Péclet Number (Pe). In the current methodology, they are defined as follows:

$$Fo = \frac{\alpha_g t}{r_b^2} \tag{2.2}$$

$$Pe = \frac{u_g r_b}{\alpha_g} \tag{2.3}$$

where α_g is the ground thermal diffusivity [$m^2 s^{-1}$], u_g is the groundwater flow velocity [$m s^{-1}$], r_b is the borehole radius [m], and t is the time [s]. The correlations also use the optimization variables H and B. This is where the computational time becomes problematic: these variables change at the end of each iteration of the optimization routine and thus, G-functions must be calculated again each time. This is why it is important to have an efficient way to do it. The general definition of G-functions is:

$$G = k_g \frac{\theta}{q'_g} \tag{2.4}$$

where θ is the average temperature change at the surface of the boreholes due to the heat input to the ground, k_g is the ground thermal conductivity and q'_g is the borefield load par unit of length.

A new function has been developed in MATLAB to use the correlation described in Section 4 of [22]. This correlation calculates a G-function for a single borehole G_1 and another one

for a borefield with multiple boreholes G_{N1}. Then, they are combined to obtain a G-function G_N that describes the heat transfer for the entire borefield, i.e.,:

$$G_N = G_1 + G_{N1} \tag{2.5}$$

The procedure to calculate G_1 is quite simple, since it can be described by two functions with asymptotic behaviors:

$$G_{1,Y}(\chi) = Y_1 + \sqrt{Y_2\chi^2 + Y_3\chi + Y_4} + \frac{Y_5}{\sqrt{Y_6\chi - Y_7}} \tag{2.6}$$

$$G_{1,Z}(\chi) = \frac{Z_1(\chi-\varepsilon)^3}{(\chi-\varepsilon)^2 + 20^{-(\chi-\varepsilon-Z_2)/Z_3} + Z_4} \tag{2.7}$$

with $\chi = \log Fo$. Empirical coefficients Y and Z have been determined by minimizing the error between the correlation and the actual value of G_1, and can be found in [22]. The coefficient ε can be computed with a summation of 10 terms depending on Pe, H, and r_b:

$$\varepsilon = \sum_{k=1}^{10} \omega_{G1,k} V_{G1,k} \tag{2.8}$$

where $\omega_{G1,k}$ is the weight associated with variable combination k and $V_{G1,k}$ is the k^{th} variable combination of Pe, H, and r_b. The terms $\omega_{G1,k}$ and $V_{G1,k}$ are shown in Table A1, in the appendix of [22].

The procedure for the calculation of G_{N1} is more complex, since it is based on a time-dependent parametric curve fitting:

$$G_{N1}(Fo) \approx \gamma\left[1 - \frac{1}{e^{(\log(Fo)-\mu)/\beta} + 1}\right] \tag{2.9}$$

where γ, β, and μ are the three parameters to fit, calculated in the following way:

$$\gamma = G_{ss} \tag{2.10}$$

$$\mu = \frac{1}{2}\left(Fo_{90\%}^{\log} + Fo_{10\%}^{\log}\right) \tag{2.11}$$

$$\beta = \frac{1}{4.4}\left(Fo_{90\%}^{\log} - Fo_{10\%}^{\log}\right) \tag{2.12}$$

An empirical estimation of these parameters must be done using a series of 64 weights ω_k and variable combinations V_k to compute G_{ss}, $Fo_{10\%}^{\log}$, and $Fo_{90\%}^{\log}$:

$$Fo_{10\%}^{\log} = \sum_{k=1}^{64} \omega_k^{Fo_{10\%}^{\log}} V_k \tag{2.13}$$

$$Fo_{90\%}^{\log} = \sum_{k=1}^{64} \omega_k^{Fo_{90\%}^{\log}} V_k \tag{2.14}$$

$$G_{ss}^1 = \sum_{k=1}^{64} \omega_k^{G_{ss}} V_k, \text{ then} \begin{cases} G_{ss}^2 = \sum_{k=1}^{64} \omega_k^{G_{ss} \le 2} V_k & \text{if } G_{ss}^1 \le 2 \\ G_{ss}^2 = \sum_{k=1}^{64} \omega_k^{G_{ss} > 2} V_k & \text{if } G_{ss}^1 > 2 \end{cases} \tag{2.15}$$

The terms ω_k and V_k are shown in Table A2, in the appendix of [22]. Six different variables are combined: the borehole depth H, the distance between two adjacent boreholes B, the total number of boreholes N, the borefield aspect ratio (longest side/shortest side) A, the Péclet number Pe, and the groundwater flow angle on the borefield ϕ. The combinations include terms from first to third order (e.g., H, H^2, and H^3).

As stated previously, computational time is an issue when developing a sizing methodology that includes an optimization approach, since many iterations are necessary to obtain the best solution. In the current methodology, all the G-functions must be calculated at the beginning of each optimization's iteration. Tests were made to measure this computational time. It was found that for a project duration of 20 years, with a time step of 1 day (7300 time steps in total), less than a second is necessary to compute all the G-functions with the correlation function, while about a second is needed for a single G-function when using the model functions. Using the correlation is therefore very appealing for the optimization approach. Note that these tests were realized with an Intel i7-3770 3.4 GHz CPU and 16 GB of RAM.

2.2.2. Challenges encountered

Unfortunately, a problem was encountered during the simulations aiming to find optimal designs for a series of projects. Strange behaviors were observed, and investigations revealed

that for certain combinations of parameters, especially for high values of Pe and Fo numbers, the correlation could yield negative values for G_{ss}, i.e., the value of G_{N1} when it reaches steady state, as seen in Figure 2.2. This was problematic because it is not physical and led the optimization away from the real optimal design.

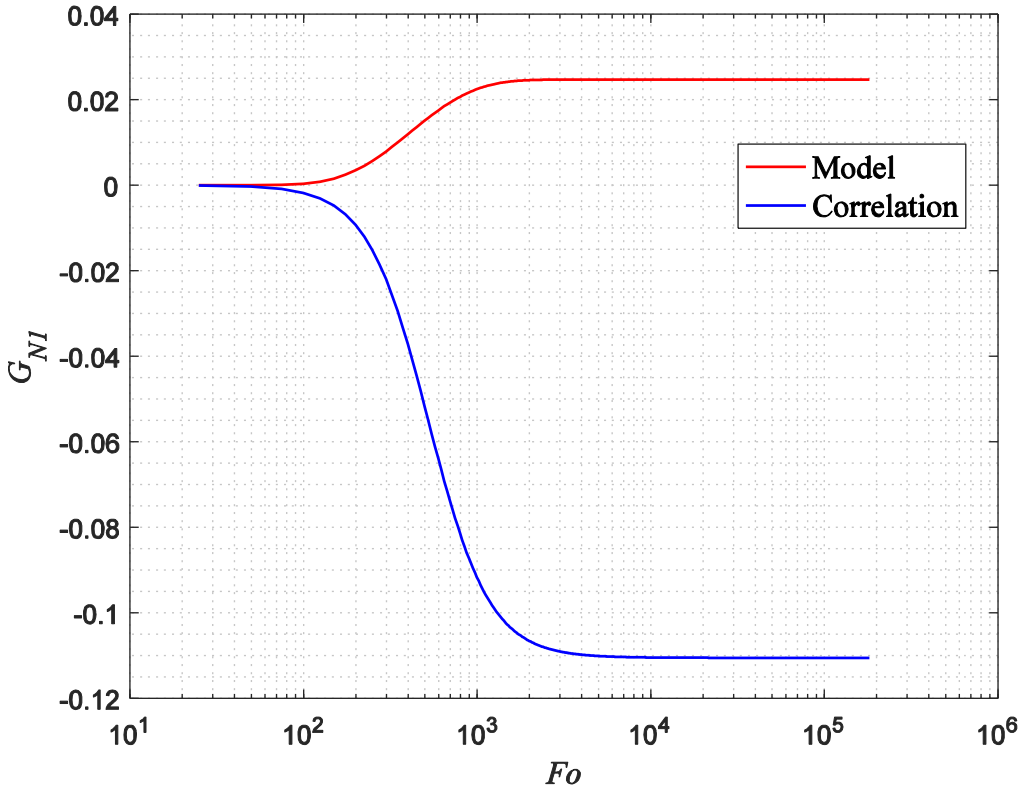

Figure 2.2: Example of incorrect behavior for G_{N1} with $Pe = 10^{-1}$, $H = 105$ m, $B = 3$ m, $N_x = 1$, $N_y = 3$, and $\phi = 0^{\circ}$

A parametric study was done to see the importance of each variable in the correlation result. A high dependence on the distance between two consecutive boreholes (B) was found for G_{ss}, so additional terms of higher order $(B^4, B^5, B^6$ and $B^7)$ were added to the existing 64 terms to improve the accuracy of the correlation. While improving the results, this did not completely solve the issue, since negative values were still sometimes computed by the correlation function. At this point, the scope of the methodology was reduced to an attempt

to produce a new correlation specifically for problematic scenarios: the number of boreholes in the x-direction was limited to 1, the angle of the groundwater flow ϕ was limited to 0°, and Pe was limited to 10^{-1}, since the problem only appeared for high flow velocities. This approach reduced the number of variables to 3 (H, B, and N_y), with 19 terms for the correlation instead of 64. Additional terms for B were also added to improve the fitting. Finally, each variable was scaled from 0 to 1 to better capture its relative influence on the new correlation. This addition did not significantly enhance the results. Figure 2.3 presents a summary of how these additions improved the fitting for G_{ss} with regards to B.

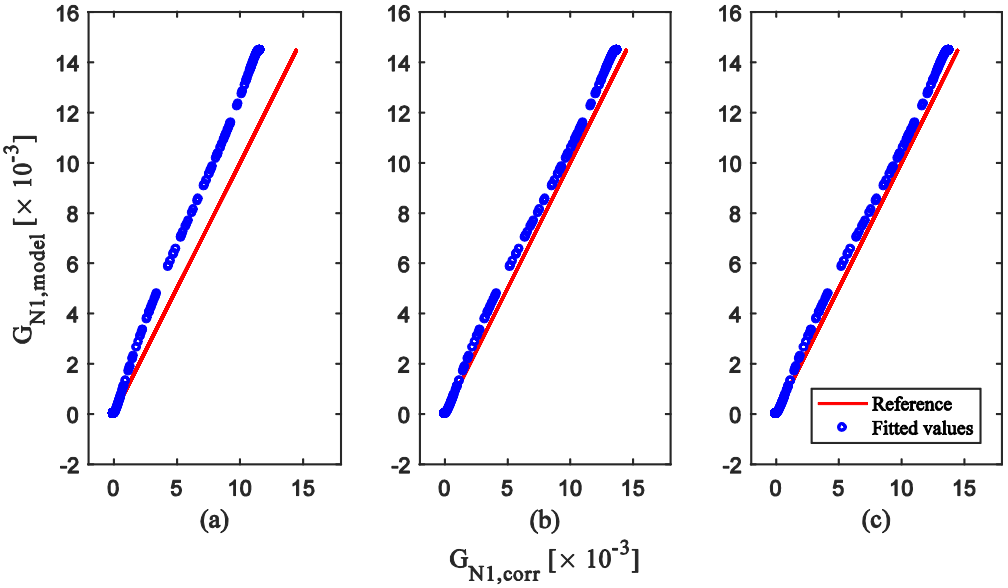

Figure 2.3: New correlation for G-functions: **(a)** reduced expression, **(b)** additional terms for B, **(c)** variable scaling added

After investigation, the problem was found to specifically occur when the model predicted $G_{ss} = 0$ for certain values of Fo. The correlation was unable to reflect this behavior with a summation of terms. The idea of developing a new correlation was therefore abandoned.

2.2.3. Solutions for G-functions

The G-functions obtained with the combination of the ICS and MFLS analytical models yield a correct estimation of the effect of groundwater flow on the borefield, but their computation is time consuming. Therefore, it was decided to calculate the G-function at 20 different times logarithmically spaced across the entire duration of each simulation (i.e., at 20 different values of the Fo number). Values of the G-functions at intermediate times were calculated by interpolating with spline functions already implemented in MATLAB, thus requiring no additional work. An example for a test scenario is presented in Figure 2.4. By comparing the interpolated and computed values, it was found that the average absolute difference was less than 0.02%. This approach is a compromise that was found to give acceptable results for G-functions within acceptable computational times. Unfortunately, the correlation developed by Tye-Gingras and Gosselin [22] was discarded in the final methodology, as the interpolation approach was deemed the best possible way to include G-functions in the methodology.

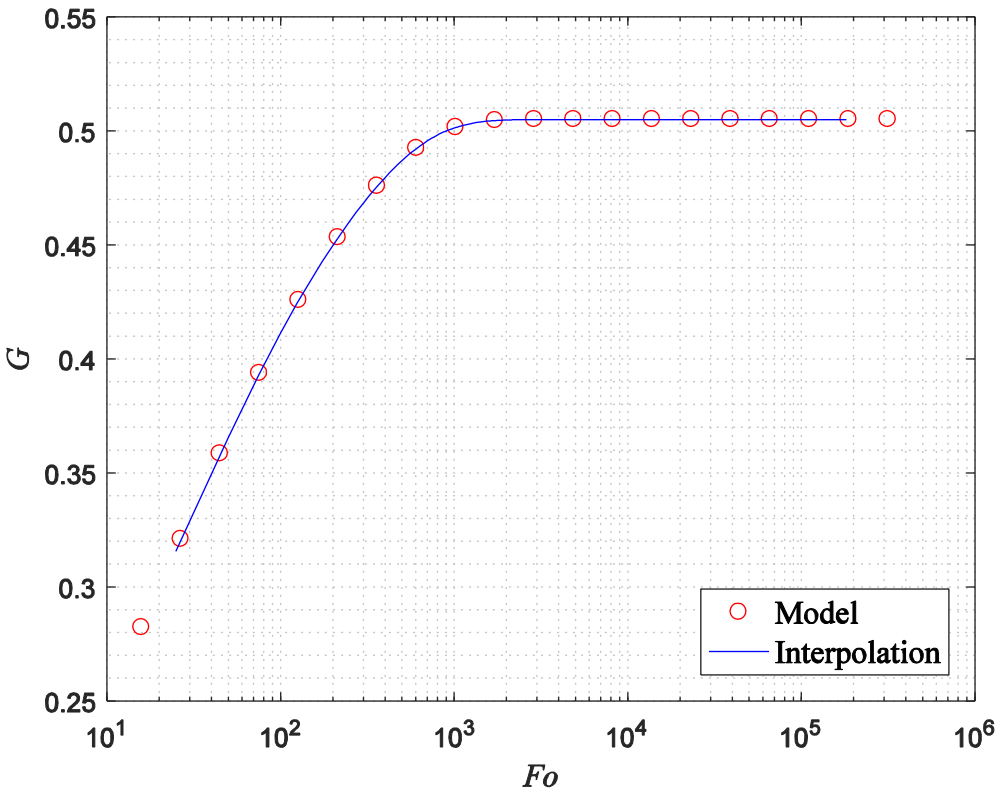

Figure 2.4: Interpolation of G-functions

2.2.4. Simplification of the computation of G-functions

In order to address the computational time issue, a review of the mathematical development of the G-functions implementation in the methodology has been done. The superposition principle can be used in conjunction with G-functions to describe the average borehole surface temperature increase or decrease after the nth pulse (θ_n) with the following equation:

$$\theta_n = \left(\frac{1}{k_g L_{GHX}}\right)\left(q_{g,n}G_1 + \sum_{i=1}^{n-1} q_{g,i}\left[G_{n-i+1} - G_{n-i}\right]\right) \qquad (2.16)$$

This temperature at a given time step is influenced by what was happened during all previous time steps and this behavior is included in the G-functions. It was discovered that if all pulses have the same duration, only the positive terms of the summation (θ_n^+) needed to be computed and that θ_n can then be calculated by using θ_{n-1}^+, i.e., θ_n^+ at the previous time step:

$$\theta_1 = \left(\frac{1}{k_g L_{GHX}} \right) \left(q_{g,1} G_1 \right) \tag{2.17}$$

$$\theta_2 = \left(\frac{1}{k_g L_{GHX}} \right) \left(q_{g,2} G_1 + q_{g,1} G_2 - \left[q_{g,1} G_1 \right] \right) \tag{2.18}$$

$$\theta_3 = \left(\frac{1}{k_g L_{GHX}} \right) \left(q_{g,3} G_1 + q_{g,1} G_3 + q_{g,2} G_2 - \left[q_{g,2} G_1 + q_{g,1} G_2 \right] \right) \tag{2.19}$$

$$\theta_4 = \left(\frac{1}{k_g L_{GHX}} \right) \left(q_{g,4} G_1 + q_{g,1} G_4 + q_{g,2} G_3 + q_{g,3} G_2 - \left[q_{g,3} G_1 + q_{g,1} G_3 + q_{g,2} G_2 \right] \right) \tag{2.20}$$

$$\theta_n^+ = \left(\frac{1}{k_g L_{GHX}} \right) \left(\sum_{i=1}^{n} q_{g,i} G_{n-i+1} \right) \tag{2.21}$$

$$\theta_n = \theta_n^+ - \theta_{n-1}^+ \tag{2.22}$$

This discovery enabled a significant time reduction, since this summation is a huge bottleneck in the MATLAB program. It must be repeated for each time step, each time with an additional term (because n is increased by 1). If the convergence criteria is not satisfied, another iteration of the energy simulation of the system is taken, thus repeating the summation. Then, this process is repeated at every iteration of the optimization routine. The simplification presented above considerably reduces computational time, and is a new addition to current methodologies using G-functions. Indeed, calculation speed tests have shown that computational time can be cut by up to 25% when using this simplification.

2.3. Testing procedure

While developing an optimization methodology, it is important to insure its robustness and the viability of its results through validation. In this section, the convergence criteria used for the energy simulation of the GCHP system will be discussed. Then, comparisons with previous results made with another sizing methodology will be presented.

2.3.1. Convergence criterion

During the energy simulation of the system, which will be described in detail in Chapter 3, the borefield outlet temperature needs to be evaluated. The accuracy of this temperature is crucial to the accuracy of the overall results, since it influences almost every parameter calculated by the energy simulation, as seen in Figure 3.1. First, it is used as a guess for the undisturbed ground temperature. Then, a new temperature is calculated by going through the procedure using this temperature as the input for a new iteration. The procedure is repeated until convergence is achieved, i.e., until $T_{f,out}$ stops changing between two consecutive iterations, using the following criterion to declare convergence at a given time step:

$$\left| 1 - \frac{N\dot{m}_f c_f \left(T_{f,in} - T_{f,out}^{new} \right)}{q_g} \right| \leq 0.001 \qquad (2.23)$$

where $\dot{m}_f$ is the mass flow rate of the fluid inside the boreholes [kg s^{-1}], c_f is the specific heat [J kg^{-1} K^{-1}], q_g is the ground thermal load [W], $T_{f,in}$ is the borefield inlet temperature [°C], and $T_{f,out}^{new}$ is the new borefield outlet temperature calculated at the current iteration of the time step. The convergence criterion of 0.001 was determined by a series of tests in which more or less stringent criteria were considered. For example, the precision of the result and the computation time were evaluated for the following parameters: $Pe = 10^{-1}$, $k = 3\,\mathrm{W m^{-1} K^{-1}}$, $\phi = 0^{o}$, $N_x = 2$, $N_y = 2$, $H = 60$ m, $B = 8$ m, $f = 60\%$, and a project duration of 20 years. The results of this test are presented in Table 2.1.

Table 2.1: Convergence criterion test for $Pe = 10^{-1}$, $k = 3\,\mathrm{Wm^{-1}K^{-1}}$, $\phi = 0^{o}$, $N_x = 2$, $N_y = 2$, $H = 60$ m, $B = 8$ m, $f = 60\%$, and a project duration of 20 years

Criterion	0.00001	0.0001	0.001	0.01	0.1
Project total cost [$]	151,814.60	151,814.57	151,814.26	151,805.82	151,726.05
Average computation time [s]	5.95	4.49	3.23	2.13	1.31

Accuracy to the nearest dollar provided by the criterion of 0.001 is satisfactory for the current methodology as it is conservative, and the average computational time is deemed acceptable for the accuracy of the project total cost that can be obtained with this criterion.

2.3.2. Relaxation factor

An under-relaxation factor (λ) was applied to the borefield outlet temperature $T_{f,out}^{new}$ calculated during the iterative procedure described in Section 3.3.4 in order to achieve convergence ($0 \le \lambda \le 1$). This factor is necessary when working with a nonlinear problem. The new temperature found for a given iteration j is used as the starting point for the calculations of the next iteration $j+1$:

$$T_{f,out}(j+1) = T_{f,out}(j) + \lambda\left(T_{f,out}^{new}(j) - T_{f,out}(j)\right) \tag{2.24}$$

For the first iteration of the first time step, $T_{f,out}$ is unknown, so it is set equal to the unperturbed ground temperature T_g as a first guess. Different values were tested for λ. Convergence was attained for all scenarios tested with $\lambda = 0.5$, so this value was used for all the simulations.

A physics-based problem was uncovered during the investigation for the under-relaxation factor for some extreme cases, particularly when the ground thermal conductivity k_g was low (i.e., $k_g \leq 1.5$ W·m^{-1}K^{-1}). The resulting system was simply too small to provide the building loads during the winter and summer peaks, even if the design variables were set to the maximum values permitted by their boundaries. Instability was observed during the peak periods, as the simulation kept alternating between the backup system and the GCHP system. The optimization routine was not programmed to give enough time to the ground for its temperature to reach acceptable values for the GCHP system to be used. Thus, convergence was barely attained by the iterative procedure, particularly if λ was too large. Correcting this unstable behavior would have taken considerable work. Fortunately, with $\lambda = 0.5$, convergence was attained within an acceptable number of iterations, which keeps the calculation time short. While the instability caused by the physics of the problem was still present, the obtained design was simply not optimal for the scenario tested, and it was rejected in the final design selection.

2.3.3. Comparison with existing results

Since the new methodology is based on that presented in [24], it is interesting to validate the new results by comparing them to previous ones. Some differences are predictable: for instance, the current methodology uses daily building loads, while the previous methodology used hourly loads. This will influence the initial and the operational costs. Also, a fraction of the maximum load for the system's cooling mode is calculated in order to achieve heat recovery in the ground during summer. In the previous methodology, the same fraction was used during both the heating and the cooling mode. This change will influence the operational cost of the GCHP system.

In order to compare project costs, a single simulation was performed with the new procedure using a set of parameters described in Table 3 of [24]: $N_x = 3$, $N_y = 2$, $k = 3$W·m^{-1}K^{-1}, $H_{opt} = 64.7$ m, $B_{opt} = 6.2$ m, and $f_{opt} = 75.6\%$. Groundwater flow velocity was set to a negligible value (i.e. 10^{-5} m/s), since the previous methodology did not consider it. The

results are presented in Table 2.2. Note that they describe the general behavior of the new methodology as compared to the previous one, and any set of parameters would have led to the same conclusions.

Table 2.2: Comparison of costs from [24] and those obtained with the new methodology for a specific scenario

	$C_{tot,\min}$ (k$)	C_a (k$)	C_{ini} (k$)	C_{HP} (k$)	C_{drill} (k$)	C_{ex} (k$)	C_{pipe} (k$)
Previous methodology	113.3	70.6	42.7	23.0	15.5	1.6	2.6
New methodology	105.9	67.1	38.9	19.1	15.5	1.6	2.6

As stated previously, due to the lower maximum load in heating, the cost of the heat pump is reduced, since it is calculated with a correlation [28] based on this maximum value:

$$C_{HP} = 1949.5 \times q_{heating,\max}^{0.665} \tag{2.25}$$

The other initial costs (C_{drill}, C_{ex}, and C_{pipe}) are calculated in the same way, thus they are identical, and the difference between the total initial costs is only about 9%. The difference in operational cost is more complex to explain, since it largely depends on the estimation of heat transfer in the ground, which differs between the two methodologies. However, one can see that the variation is only about 5%, which is acceptable in this situation considering the differences between the two methodologies.

CHAPTER 3 INFLUENCE OF GROUNDWATER FLOW ON COST MINIMIZATION OF GROUND COUPLED HEAT PUMP SYSTEMS

Résumé

Ce chapitre présente une nouvelle méthodologie de dimensionnement pour les systèmes de pompe à chaleur géothermique (PAC) qui tient compte des écoulements souterrains (en utilisant des fonctions G basées sur des modèles analytiques) afin de réaliser une optimisation économique du coût total du projet. La procédure comprend le calcul des coûts initiaux et opérationnels. Des variables de conception optimales (profondeur de forage, distance entre les puits consécutifs, etc.) et des aménagements de champ de puits (nombre de puits dans la direction *x*) sont présentés pour différentes valeurs de conductivité thermique du sol. En outre, une étude paramétrique est effectuée pour mesurer l'impact de la vitesse et de l'angle de l'écoulement des eaux souterraines par rapport au champ de puits sur l'aspect économique du projet. Il est démontré que les effets de la vitesse d'écoulement des eaux souterraines sur le coût total n'apparaissent que pour des vitesses élevées, c'est-à-dire $Pe \gtrsim 10^{-2}$. D'autre part, l'angle d'écoulement des eaux souterraines est peu influent, quelle que soit la vitesse d'écoulement de l'eau souterraine, c'est-à-dire que le gain économique net qui peut être obtenu en choisissant l'orientation optimale est beaucoup plus petit par rapport au coût total du système (moins de 2%). Une comparaison simultanée des coûts initiaux et opérationnels montre que pour toutes les valeurs de Pe, les coûts initiaux plus élevés entraînent généralement des coûts opérationnels plus faibles. Enfin, les conceptions optimisées sont testées en dehors des conditions d'opération nominales. On peut observer que les conséquences économiques de l'exploitation hors des conditions nominales sont bien pires si la vitesse de l'écoulement des eaux souterraines est surestimée, ce qui peut entraîner une augmentation des coûts opérationnels de 5,8%. Une mauvaise estimation de l'angle d'écoulement pendant la phase de conception, cependant, entraîne seulement une augmentation des coûts opérationnels d'au plus 2,4% pour les cas considérés dans ce chapitre.

Abstract

This chapter introduces a new sizing methodology for ground coupled heat pump (GCHP) systems which takes into account groundwater flow (by using G-functions based on analytical models) in order to achieve an economic optimization of the total cost of the project. The procedure includes the calculation of the initial and the annual operational costs. Optimal design variables (borehole depths, distance between adjacent boreholes, etc.) and borefield layouts (number of boreholes in the x-direction) are presented for different values of the thermal conductivity of the ground. In addition, a parametric study is completed to measure the impact of the groundwater flow velocity and angle with respect to the borefield on the economics of the project. It is shown that the effects of the groundwater flow velocity on total cost become apparent only for high velocities, i.e., $Pe \gtrsim 10^{-2}$. On the other hand, the groundwater flow angle has less impacts regardless of the groundwater flow velocity, i.e., the net economic gain that can be obtained by choosing the optimal orientation is much smaller compared to the total cost of the system (less than 2%). A simultaneous comparison of the initial and operational costs shows that for all Pe values, higher initial costs usually result in lower operational costs. Finally, optimized designs are tested under off-design operating conditions. It can be observed that the economic consequences of operating under off-design conditions are far worse if the groundwater flow velocity is overestimated, which can lead to an increase of the operational costs as much as 5.8%. A wrong estimation of the flow angle in the design phase, however, only leads to an increase of the operational costs of at most 2.4% for the cases considered in this chapter.

3.1. Introduction

Ground coupled heat pump systems are an interesting option for heating and cooling buildings, since they provide energy savings and have low environmental impacts compared to other systems [11], [12]. They are particularly attractive for projects in which both cooling and heating are needed, which is the case for a large variety of buildings in Canada [8]. Vertical heat exchangers, or boreholes, are the most widely used configuration in Canada. Despite their clear advantages, the main obstacle to the installation of such systems is the high investment required, which can be prohibitive. Thus, an efficient sizing methodology is needed to avoid undersized or oversized designs which can lead to a reduction of the energy savings or an increase of the initial cost.

Current sizing procedures are based on finding the required total borehole length for specified heating and cooling loads [23]. Recent studies, on the other hand, have proposed another approach to the GCHP system sizing problem by identifying the design minimizing the total cost of the system (including purchase cost and cost of operation) [24], [25]. Such an approach has the advantage of identifying the optimal fraction of the building thermal loads to be supplied by the GCHP rather than imposing this fraction.

In these sizing calculations, the ground is usually simplified and represented by a homogeneous medium in which conduction is the only heat transfer mechanism. However, groundwater is commonly found in many geological environments. Groundwater flow can significantly affect heat transfer around boreholes [3], [29], [4]–[6], and many analytical models have been developed to quantify its effects [15]–[17], [19], [30]. Previous studies have also developed relatively fast heat transfer computational methodologies with groundwater flow, such as calculating a thermal ground resistance [14] or a thermal conductivity [31], using fast Fourier transforms combined with cubic splines [32], or correlations with G-functions based on analytical models for groundwater flow [33].

Given the influence of groundwater flow on GCHP systems [18], [20], [21], [34] and the advantages of a design method based on cost minimization, this chapter introduces a new sizing methodology that takes into account groundwater flow. The total cost is in fact composed of the initial and operational costs, which both depend on different design parameters and are influenced by groundwater flow. The GCHP system that is optimized in the present chapter is introduced in Section 3.2. The methods used to calculate the total cost of the system and the energy output of the GCHP are described in Sections 3.2 and 3.3, respectively. The optimization strategy and numerical model are detailed in Section 3.4, whereas the results of the different optimization runs and their implications in terms of design strategies are discussed in Section 3.5.

3.2. Cost estimation

The general layout of the geothermal system studied in this chapter is presented in Figure 1 of [24]. The system consists of grids of N_x by N_y equally spaced boreholes in the x and y directions, respectively. The total number of boreholes N is thus given by:

$$N = N_x N_y \tag{3.1}$$

Boreholes in the *x*-direction are connected in parallel and linked together through the final column in the *y*-direction. It is assumed the all boreholes experience the same fluid mass flow rate via balancing valves. The borefield inlet and outlet pipes are connected to a circulating pump and to a heat pump, the latter being used for the heating or cooling of the building.
The total cost of the ground coupled heat pump system project is achieved by summing the initial cost of the installation and the annual operating costs, which are then converted to their present values:

$$C_{tot} = C_{ini} + \sum_{i=1}^{n} C_{a,i} \left(1+ j\right)^{-i} \tag{3.2}$$

where n is the number of years of the project, j is the interest rate [%], and $C_{a,i}$ are the annual operating cost for years 1 to n. An interest rate of 6% has been used for every simulation presented in this chapter.

3.2.1. Initial cost

The initial cost is obtained by summing the costs of the heat pump, drilling, excavation and piping:

$$C_{ini} = C_{HP} + C_{drill} + C_{ex} + C_{pipe} \tag{3.3}$$

A correlation developed by [35] is used to evaluate the heat pump cost as a function of its design load capacity:

$$C_{HP} = 1949.5 \times q_{heating,\max}^{0.665} \tag{3.4}$$

where $q_{heating,\max}$ is the maximum heating load supplied by the heat pump [kW]. Note that the prices used in this section have been taken from [24]. Drilling cost depends on the number of boreholes in the field and on their depth H. A drilling price per meter $X_{drill} = 40$ \$/m is assumed, which gives:

$$C_{drill} = N_x N_y H X_{drill} \tag{3.5}$$

Excavation cost also depends on the number of boreholes and on the distance between consecutive boreholes B. A trench is needed for every row in the *x*-direction to link boreholes together, with an additional trench to join rows in the *y*-direction. Assuming an excavation price per meter $X_{ex} = 42$ \$/m, the excavation cost can be evaluated:

$$C_{ex} = \left[N_y \left(N_x B \right) + N_y B \right] X_{ex} \tag{3.6}$$

To determine the piping cost, the total piping length L_{pipe} [m] must be evaluated. L_{pipe} is related to the number of boreholes and the distance between them, and can be estimated as follows:

$$L_{pipe} = 2\left[N_y N_x B + N_y B + N_y N_x H \right] \tag{3.7}$$

In order to simplify the model, a representative price per meter $X_{pipe} = 3$ \$/m is used, even if the diameter of each pipe used in the field might be different, since pipe diameters are usually of the same order of magnitude in GCHP systems. The piping cost can then be evaluated with the following expression:

$$C_{pipe} = L_{pipe} X_{pipe} \tag{3.8}$$

3.2.2. Operating cost

The operating cost is mostly governed by the energy consumption of the heat pump, the heat transfer fluid circulation pump and the backup heating/cooling system as seen in [24].
The instantaneous power requirement needed by the heat pump is:

$$\dot{w}_{HP}(t) = q_{HP}(t) / COP_{HP}(t) \tag{3.9}$$

where q_{HP} is the building heating load provided by the geothermal heat pump and COP_{HP} is its coefficient of performance, both detailed in Section 3.3.

The power required for the backup system is determined by subtracting the heating requirement provided by the geothermal system from the total building load, assuming $COP_{backup} = 1$ for the backup system:

$$\dot{w}_{backup}(t) = q_{build}(t) - q_{HP}(t) \tag{3.10}$$

where q_{build} is the total building load, also detailed in Section 3.3.
Finally, based on the system geometry, the power required for fluid circulation is estimated as follows:

$$\dot{w}_{pump} = 2\left[N_y N_x \left(\frac{\Delta P' H \dot{m}_f}{\rho_f} \right) + N_y \sum_{i=1}^{N_x} \left(\frac{\Delta P' B (i \dot{m}_f)}{\rho_f} \right) + \sum_{i=1}^{N_y} \left(\frac{\Delta P' B (i N_x \dot{m}_f)}{\rho_f} \right) \right] \tag{3.11}$$

where $\Delta P'$ is the head loss per unit length of piping, $\dot{m}_f$ is the fluid mass flow rate in the boreholes, and ρ_f is the fluid density.

Combining Eqs. (3.9)-(3.11), the total power requirement at a given time is:

$$\dot{w}_{tot}(t) = \dot{w}_{HP}(t) + \dot{w}_{backup}(t) + \dot{w}_{pump} \tag{3.12}$$

The evaluation of energy cost was based on local rates (Hydro-Quebec business rate "G") for which monthly energy consumption is considered [36]. Therefore, the total power requirement given by Eq. (3.12) is integrated over a month to obtain the monthly energy consumption:

$$w_{tot} = \int \dot{w}_{tot}(t) dt \tag{3.13}$$

It can be noted that the monthly cost of energy changes after the first 15,090 kWh:

$$C_{energy,i} = \begin{cases} w_{tot,i} X_{E1} & if\ w_{tot,i} \le 15.09 kWh \\ 15.09 \times 10^6 X_{E1} + \left(w_{tot,i} - 15.09 \times 10^6 \right) X_{E2} & if\ w_{tot,i} > 15.09 kWh \end{cases} \quad (3.14)$$

where X_{E1} is the energy price of the first 15,090 kWh per month and X_{E2}, the energy price of the remaining kWh per month. For the simulations presented in this chapter, $X_{E1} = 0.0878$ \$/kWh and $X_{E2} = 0.0485$ \$/kWh have been used. For each month of the simulation, if the maximum power requirement $w_{peak,i}$ exceeds 50 kW, an extra fee must be paid for that power peak [36]:

$$C_{peak,i} = \begin{cases} 0 & if\ w_{peak,i} < 50 kW \\ w_{peak,i} X_P & if\ w_{peak,i} > 50 kW \end{cases} \quad (3.15)$$

The charge for demand exceeding 50 kW (X_P) used in the present work is 15.54 \$/kW. Combining Eqs. (3.14) and (3.15), the annual operating cost can be obtained:

$$C_a = \sum_{i=1}^{12} \left(C_{energy,i} + C_{peak,i} \right) \quad (3.16)$$

Note that the different prices presented in this section were those in effect in 2013. This choice was made to facilitate comparison with previous related work (e.g., [24]), and because this chapter is focused on the development of the sizing methodology which is not affected by the year at which costs are estimated. In future work or sizing tools based on the present approach, prices could be adapted to reflect their evolution.

3.3. Energy simulation of the system

In order to evaluate the operating cost of the geothermal heat pump system discussed in the previous section, an energy simulation of the system is required. The overall simulation procedure is illustrated in a flowchart (see Figure 3.1). The objective of the simulation is to determine the heating and cooling provided to the building by the geothermal heat pump system over the timeframe considered. All relevant parameters are presented in Table 3.1.

Table 3.1: List of parameters for the energy simulations

Parameters	Values	Units
Borehole radius r_b	0.075	m
Borehole thermal resistance R_b' for: heating	0.1076	m K W^{-1}
cooling	0.1082	m K W^{-1}
Ground thermal diffusivity α_g	1.62×10^{-6}	m^2 s^{-1}
Fluid specific heat c_f	4190	J kg^{-1} K^{-1}
Fluid mass flow rate $\dot{m}_f$ in each borehole	0.2	kg s^{-1}
Head loss by unit length of piping $\Delta P'$	0.4	kPa m^{-1}
Initial ground temperature T_g	7	°C
Annual load unbalance A	-18.0	kW
Half-amplitude of annual load variation B	43.5	kW
Nominal COP for heat pump heating mode	3.5	-
Nominal COP for heat pump cooling mode	3.5	-
Correlation coefficients for heating mode, k_0, k_1, k_2	1.00000000×10^{0}	-
	1.55970900×10^{-2}	-
	-1.59310000×10^{-4}	-
Correlation coefficients for cooling mode, k_0, k_1, k_2	1.53105836×10^{0}	-
	-2.29609500×10^{-2}	-
	6.87440000×10^{-5}	-

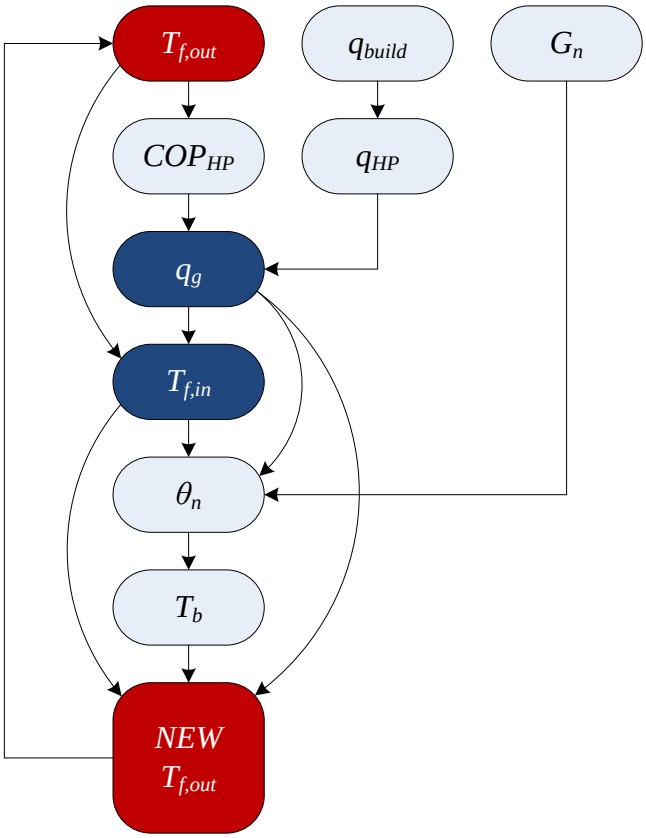

Figure 3.1: Overall simulation procedure

3.3.1. Heating and cooling needs of the building

In the present work, the total heating and cooling needs of the building are represented by a synthetic load profile:

$$q_{build}(t) = A - B\cos\left(\frac{t}{365}2\pi\right) \tag{3.17}$$

where t is the time in days, A controls the annual load unbalance and B, the half-amplitude of annual load variation. The constants A and B used in the present study are given in Table 3.1. Note that this profile gives a set of daily pulses, i.e., the heating or cooling loads needed by the building at each day of the simulation, as shown in Figure 3.2. More detailed profiles (e.g., hourly profiles) could have been used, but given how the building load is managed by the geothermal system (see next paragraph), this would only have a marginal impact.

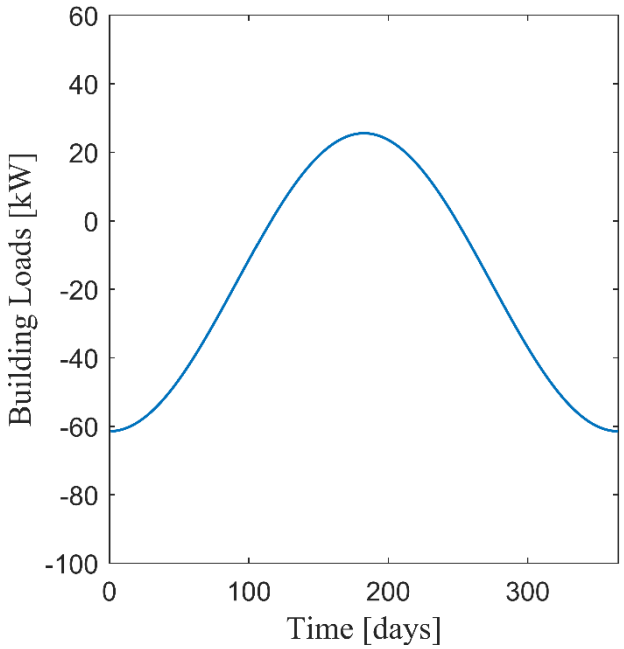

Figure 3.2: Synthetic building load profile used for simulations (negative values are heating loads, positive values are cooling loads)

Medium to large geothermal heat pump systems installed in North America are usually not designed to provide the entire heating and cooling needs. This would require too large a system to meet the peak loads for only a limited number of days per year. Instead, geothermal systems are typically used to meet a relatively constant heat transfer rate corresponding to a certain fraction f of the maximum load $q_{\max}$, in such a way that it "shaves" the actual profile given by Eq. (3.17). The remaining portion of the heating/cooling need is satisfied by a backup system:

$$q_{HP} = \begin{cases} q_{build} & if\ q_{build} < fq_{\max} \\ fq_{\max} & if\ q_{build} \geq fq_{\max} \end{cases} \tag{3.18}$$

$$q_{backup} = q_{build} - q_{HP} \tag{3.19}$$

Note that in this work, the fraction f is applied to the heating load, which is dominant most of the time in Canada, and the heat pump was sized accordingly. When the heat pump is in cooling mode, the building load is also "shaved" but with a fraction that approximately eliminates annual thermal imbalance in the ground (i.e., the yearly amount of heat discharged

in the ground is equal to the yearly amount of heat recovered from the ground). For a given value of f, this was determined by using nominal COP values for heating and cooling (see Table 3.1) and then by varying the fraction of shaving during the cooling mode ($f_{cooling}$) until a yearly thermal balance was reached or until all the cooling load is fully satisfied.

In order to keep the computational time within an acceptable range, and because of the peak "shaving" strategy described above, it was decided to use daily loads (see Figure 3.2) instead of hourly loads. For example, for a simulation over 20 years, instead of having 175,200 hourly pulses to simulate, the number of pulses is thus reduced to 7300.

3.3.2. Heat pump modeling

The heat pump allows transferring heat from the building to the ground or vice versa. Its performance is dictated by the temperature of the fluid leaving the borefield (or entering the heat pump). As shown in Figure 3.1, the fluid temperature at the outlet of the borefield ($T_{f,out}$) is used to calculate the coefficient of performance of the heat pump (COP_{HP}). This is achieved by using the following correlation found in [37]:

$$COP_{HP} = COP_{nominal}\left(k_0 + k_1 T_{f,out} + k_2 T_{f,out}^2\right) \tag{3.20}$$

where COP_{HP} is the actual COP of the heat pump and $COP_{nominal}$ is the nominal COP of the heat pump measured at standard rating conditions (e.g., 0°C for heating and 25°C for cooling). The constants used in this correlation (k_0, k_1, and k_2) change depending on whether the heat pump is in heating or cooling mode. The values that were used are those of [37] and are listed in Table 3.1.

The heating or cooling loads supplied by the borefield are determined from the COP_{HP} and the heat pump loads q_{HP}:

$$q_g = q_{HP}\left(1 \pm \frac{1}{COP_{HP}}\right) \tag{3.21}$$

where the sign is positive for cooling and negative for heating. Since COP_{HP} depends on the fluid temperature which is unknown, the actual heat transferred from or to the ground is unknown, although the building load is known.

3.3.3. Ground and fluid temperature calculation

G-functions developed in [33] were used in the present study. They relate the average temperature change (θ) at the surface of the boreholes to the heat input to the ground:

$$G = k_g \frac{\theta}{q'_g} \tag{3.22}$$

where k_g is the ground thermal conductivity and q'_g is the borefield load par unit of length, i.e., $q'_g = q_g / L_{GHX}$ with L_{GHX} the total ground heat exchanger length, which is simply the depth of a single borehole H multiplied by the total number of boreholes N. The G-functions from [33] take into account the groundwater flow velocity (u_g) and direction (ϕ), the number of boreholes (N) and their arrangement, the radius (r_b) to depth (H) ratio, the radius to spacing (B) ratio and the duration of the applied heat input. These G-functions have been validated for $Pe \leq 10^{-1}$. The flow direction is calculated from the difference between the flow axis and the *x*-axis, assuming that the angle ϕ is equal to 0 when to flow is in the *x*-direction. For the sake of illustration, an example of the steady-state G field in a borefield with groundwater flow is presented in Figure 3.3 for $\phi = 0^o$ and $\phi = 90^o$. This corresponds to the steady-state difference of temperature relative to the unperturbed ground temperature normalized with the ground conductivity and heat input. These fields were obtained from 2D finite volume simulations to illustrate the steady-state temperature field in the presence of groundwater flow, using $Pe = 10^{-1}$ and $B / r_b = 13.33$. Figure 3.3 illustrates that the thermal interactions between boreholes are affected by groundwater flow.

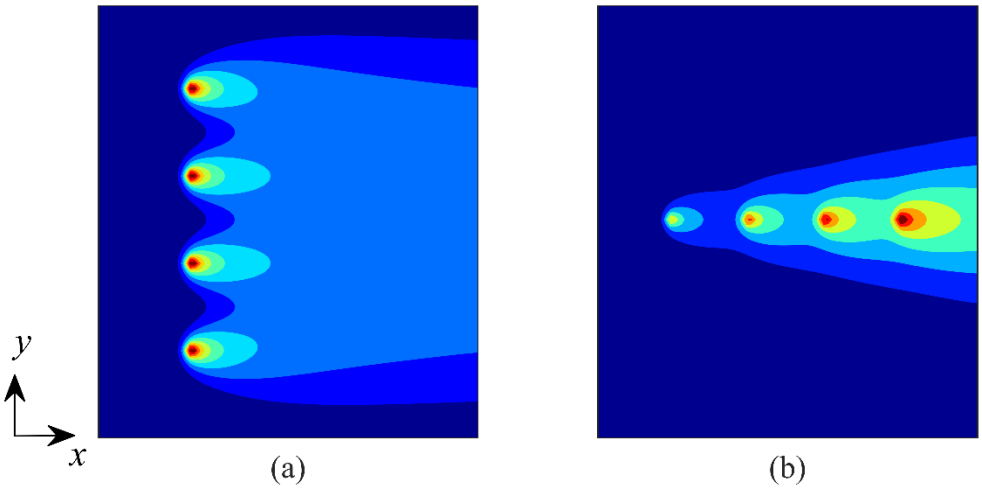

Figure 3.3: Example of steady-state G-function profile from finite volume simulations with $Pe = 10^{-1}$ and $B/r_b = 13.33$ with: **(a)** borefield axis perpendicular to the flow axis $(\phi = 0^{o})$ and **(b)** borefield axis parallel to the flow axis $(\phi = 90^{o})$

As discussed in [33], the G-functions can be estimated either through a moving finite line source (MFLS) model, an infinite cylindrical source (ICS) model, or from correlations based on these models. However, it was found during the parametric study performed in the present work that correlations could yield negative values for the G_{N1} functions in some cases (especially for high values of Pe and Fo numbers) which, in turn, resulted in an erroneous estimation of the total cost of the system. Therefore, an alternate approach was used in the present work, where combinations of the ICS and MFLS analytical models were used to calculate the G-functions at 20 different times logarithmically spaced across the entire duration of each simulation (i.e., at 20 different values of the Fo number). Values of the G-functions at intermediate times were calculated by interpolating with spline functions. This methodology considerably reduces the computational time while giving accurate results for the G-functions. It was found that the average absolute difference between the interpolated G-functions at intermediate times and those computed with the model was less than 0.02%. As discussed in [38], the superposition principle can be used in conjunction with G-functions to describe the average borehole surface temperature evolution. This temperature at a given time step is influenced by what happened during all previous time steps.

Due to the linearity of the problem, the superposition principle may be used to calculate the average borehole surface temperature increase or decrease after the nth pulse with the help of the following equation:

$$\theta_n = \left(\frac{1}{k_g L_{GHX}} \right) \left(q_{g,n} G_1 + \sum_{i=1}^{n-1} q_{g,i} \left[G_{n-i+1} - G_{n-i} \right] \right) \tag{3.23}$$

In order to further reduce the computational time, it is possible to show that if all pulses have the same duration, only the positive terms of the summation (θ_n^+) need to be computed, and that θ_n can then be calculated by using θ_{n-1}^+, i.e., θ_n^+ at the previous time step:

$$\theta_n^+ = \left(\frac{1}{k_g L_{GHX}} \right) \left(\sum_{i=1}^{n} q_{g,i} G_{n-i+1} \right) \tag{3.24}$$

$$\theta_n = \theta_n^+ - \theta_{n-1}^+ \tag{3.25}$$

For the first iteration, θ_{n-1}^+ does not exist and θ_1 is simply:

$$\theta_1 = \theta_1^+ = \frac{q_{g,1}}{k_g L_{GHX}} G_1 \tag{3.26}$$

One can relate the borehole surface temperature to the temperature of the fluid circulating in the borefield via the borehole thermal resistance:

$$q_g' = \frac{\left(\bar{T}_f - T_b \right)}{R_b'} \tag{3.27}$$

where R_b' is the borehole thermal resistance per unit of length, T_b is the borehole surface temperature and $\bar{T}_f$ is the fluid temperature in the boreholes, assumed to be :

$$\bar{T}_f = \frac{\left(T_{f,in} + T_{f,out} \right)}{2} \tag{3.28}$$

where $T_{f,in}$ is the temperature of the fluid entering the borefield and $T_{f,out}$ is the temperature of the fluid exiting the borefield. In the present work, the borehole resistance was calculated with shape factors described in [39].

3.3.4. Iterative procedure

This section describes how the different elements of the previous sections were assembled to perform the energy simulation. At a given time step, the temperature of the water exiting the borefield and entering the heat pump ($T_{f,out}$) is unknown and an iterative process was thus implemented to calculate this temperature. For the first iteration of the first time step, this temperature is set equal to the unperturbed ground temperature (T_g). For the other time steps, the temperature of the previous time step was used as a guess.

The effective COP of the heat pump for the guessed fluid temperature can be calculated with Eq. (3.20), and then the actual heat load to the ground can be estimated with Eq. (3.21). Assuming no heat loss or gain between the heat pump and the boreholes, the temperature of the water entering the borefield ($T_{f,in}$) is calculated, based on energy conservation:

$$T_{f,in} = \frac{q_g}{N\dot{m}_f c_f} + T_{f,out} \tag{3.29}$$

The G-functions introduced previously describe the heat transfer in the entire borefield. Since G-functions do not change between two consecutive iterations, they can be all calculated before beginning the iterative procedure. Afterwards, the average surface temperature of all boreholes (T_b) at the nth time step is calculated with the unperturbed ground temperature and the average temperature change at the surface of the boreholes:

$$T_b = T_g + \theta_n \tag{3.30}$$

The exiting water temperature for the borefield can now be determined by combining Eqs. (3.27) and (3.28), assuming that the fluid in the boreholes is at the temperature $\bar{T}_f$:

$$T_{f,out}^{new} = 2\left(q_g' R_b' + T_b - \frac{T_{f,in}}{2} \right) \tag{3.31}$$

$T_{f,in}$ is provided by Eq. (3.29) and T_b is provided by Eq. (3.30). This new value of $T_{f,out}$ is compared to the guessed value. As long as it is different from the guess, it is used as the input for a new iteration. The procedure is repeated until convergence is achieved, i.e., until $T_{f,out}$

stops changing between two consecutive iterations. The following criterion was used to declare convergence at a given time step:

$$\left| 1 - \frac{N\dot{m}_f c_f \left(T_{f,in} - T_{f,out}^{new} \right)}{q_g} \right| \leq 0.001 \qquad (3.32)$$

More stringent convergence criteria were considered, but did not yield significant changes to the results: the calculation time was longer, but the results were nearly identical. Once the final exiting water temperature is found for the first time step, the whole procedure is repeated for every time step, using the previous $T_{f,out}$ as the starting point for the calculations.

Finally, it is worth mentioning that in order to avoid non-physical behavior, constraints were applied to the numerical model. For instance, since the COP of the heat pump is calculated from a correlation, some input parameters could be out of its range of validity, which could result in erroneous COP values and non-physical results. To prevent this from happening, a constraint was applied to COP_{HP} such that it could not assume a value lower than unity, because such a value would indicate a system less efficient than the backup system. In this case, COP_{HP} was set to 1, q_g was set to 0 W, and it was assumed that only the backup system was used.

3.4. Optimization strategy

The goal of the optimization procedure is to find the best GCHP system design for a given building load. The lowest total cost of the project is defined by minimizing the objective function. A two-steps optimization procedure was implemented. First, a borefield layout was specified (i.e, N_x and N_y) and three continuous variables were optimized with the MATLAB optimization function "*fmincon*", a nonlinear solver [27]. These three variables are: the depth of the boreholes (H), the distance between adjacent boreholes (B), and the fraction of the maximum load assumed by the geothermal heat pump system (f). The bounds of these variables are presented in Table 3.2. It was found that the total cost design space defined by H, B and f was fairly large and contained several local minima. In order to prevent the optimization process from converging towards local optimal designs, 27 different starting

points for the optimization routine were used, i.e., 3 different starting values for each of H, B and f (lower and upper boundaries, and mid-range value).

The optimization of the three continuous variables was then repeated, this time with a different layout. By considering several possible values of N_x and N_y, it was thus possible to identify the best layout along with the best values of H, B and f. This two-step approach was chosen because N_x and N_y are discrete variables which are not easily dealt with in "*fmincon*". In this chapter, borefield layouts ranging from 1×1 to 1×9 were studied, i.e., N_x was set to 1 and only N_y could vary, representing, for example, a layer of terrain available for digging boreholes. The methodology could easily be used for other sets of layouts. The two-step optimization procedure was applied to different scenarios involving different values of ground thermal conductivity k_g, Péclet number Pe (which depends on the groundwater flow velocity u_g), groundwater flow angle (ϕ), and duration of the project (n). The range of these parameters investigated in this chapter is also shown in Table 3.2.

Table 3.2: Bounds of design variables (H, B, f, N_x, N_y) during the optimization and range of parameters (k_g, Pe, ϕ, n) investigated

Variables	Lower	Upper	Units
Depth of the boreholes H	45	105	m
Distance between adjacent boreholes B	3	8	m
Fraction of the maximum load f	50	90	%
Number of boreholes in *x*-direction N_x	1	1	-
Number of boreholes in *y*-direction N_y	1	9	-
Ground thermal conductivity k_g	1	4	W m^{-1} K^{-1}
Péclet number Pe	10^{-4}	10^{-1}	-
Groundwater flow angle ϕ	0	90	°
Duration of the project n	5	40	years

3.5. Results and discussion

In this section, the results of the optimization technique combined with the energy model and cost estimation described in the previous sections are presented. First, the minimized total cost of the GCHP system for different values of ground thermal conductivity and groundwater flow velocity is presented in Section 3.5.1. Then, the impact of the groundwater flow angle and the consequences of the project duration on the minimized total cost are assessed in Sections 3.5.2 and 3.5.3, respectively. Finally, in order to demonstrate the impact of neglecting groundwater flow on the operational costs of a GCHP system, simulations were performed using designs that were optimized under a certain Pe condition, but by using them under different operating conditions, which is discussed in Section 3.5.4.

3.5.1. Impact of ground thermal conductivity and groundwater flow velocity

In order to assess the impact of the groundwater flow velocity on the total cost of a GCHP system, a series of optimization runs were performed for a project duration of 20 years and under the assumption that the groundwater flow was perpendicular to the borefield grid, i.e., $\phi = 0^{o}$. Borefield layouts ranging from 1×1 to 1×9 were simulated for 7 values of k_g ranging from 1 to 4 W m^{-1} K^{-1} and 4 values of Pe ranging from 10^{-4} to 10^{-1}. For each combination of the aforementioned parameters, the borehole depth H, the distance between adjacent boreholes B, and the borefield utilization fraction f were optimized with the aim of minimizing the total cost of the system. The layout yielding the smallest cost and its corresponding optimized values of H, B and f was considered as the "optimal" design for the particular values of k_g and Pe. It should be noted that in many cases, due to the thermal imbalance of the load, $f_{cooling}$ often reaches 100%, i.e., the heat pump is large enough to provide the entire cooling load for the building. The overall best results for each optimization run (designs with the lowest total cost) are depicted in Figure 3.4. In addition, a summary of the overall best layouts for each combination of k_g and Pe is presented in Table 3.3.

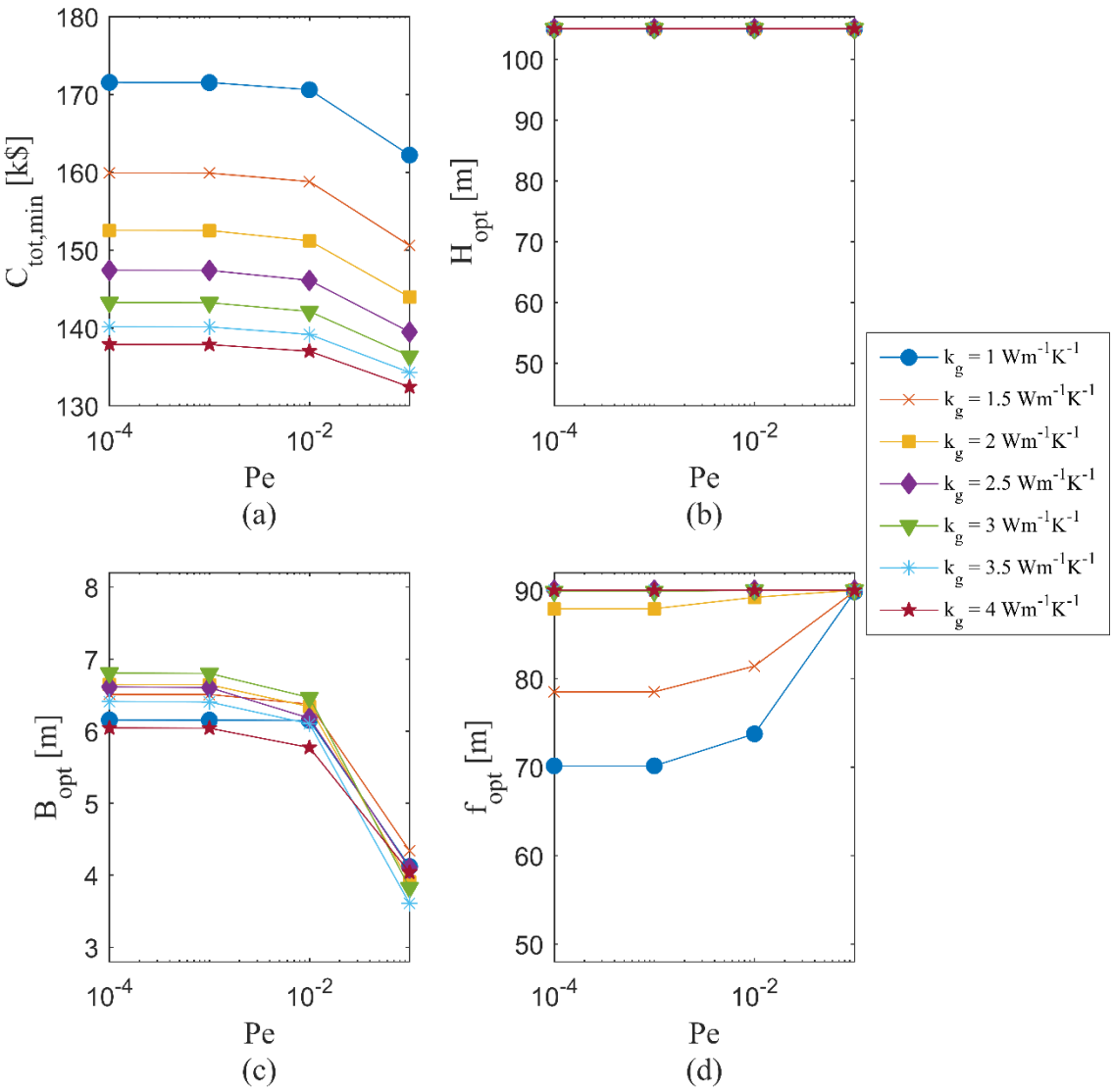

Figure 3.4: Effect of Péclet number and ground thermal conductivity on: **(a)** minimum total cost, **(b)** optimal borehole depth, **(c)** optimal distance between adjacent boreholes and **(d)** optimal fraction of maximum load

By looking at Figure 3.4a, it can first be observed that the thermal conductivity of the ground k_g has a strong effect on the total cost of the GCHP system. Indeed, higher values of k_g allow a better heat transfer between the ground and the borefield. Therefore, the system can be designed to rely more on the GCHP than on the backup system and thus the operational cost is reduced, which results in a cheaper system. This can be seen in Figure 3.4d, where the optimal fraction of the load assumed by the GCHP system increases as k_g increases. This result is in accordance with previous observations, for example see [24]. The value of k_g has an impact on the optimal distance between boreholes, but mostly when Pe is small, i.e., for cases in which conduction is the dominant mode of heat transfer in the ground, as can be seen in Figure 3.4c. It is hard to identify a clear trend with respect to k_g since all points in Figure 3.4 have different optimal loads and borefield layouts.

The impact of Pe is also visible in Figure 3.4. For increasing values of Pe, convective heat transfer becomes more and more significant. This phenomenon becomes more apparent for Pe values greater than 10^{-2}. Typically, Pe numbers of that order of magnitude can only be found under specific conditions, as discussed in [40]. However, the impact of groundwater flow is clearly visible in Figure 3.4. For example, it can be observed in Figure 3.4a that for high values of Pe, optimal designs have a lower total cost. For example, at $Pe = 10^{-1}$, the optimized design is 5.8% cheaper than at $Pe = 10^{-4}$ when $k_g = 1.5$ W m^{-1} K^{-1}. Groundwater flow tends to lower the value of the G-function, in particular for long timeframes, thus promoting the heat transfer in the borefield [33] and reducing the operational cost, which leads to a cheaper system. This result could be expected since the importance of convective heat transfer along the boreholes is directly connected to the magnitude of the groundwater flow velocity. Since a faster flow means better convective heat transfer along the boreholes, the result is a higher $T_{f,out}$ and a higher COP_{HP} (i.e., Eq. (3.20)), and operational costs can be directly correlated to COP_{HP}, see Eqs. (3.9), (3.12)-(3.16). As a result, the optimal fraction of the load assumed by the GCHP system increases with Pe in Figure 3.4d.

Furthermore, another source of savings in the presence of groundwater flow comes from the fact that the zone thermally influenced by each borehole shrinks as Pe increases, thus boreholes can be closer to each other without increasing the impact of thermal interactions. Therefore, one can see in Figure 3.4c that B_{opt} tends to decrease with Pe. This slightly reduces the piping, excavation and pumping costs. By looking at Figure 3.4b, one can see that the maximum value for H_{opt} was always selected for every combination of k_g and Pe. The high drilling cost associated with deeper boreholes were compensated by the savings on the operational cost, for the scenarios tested in this chapter.

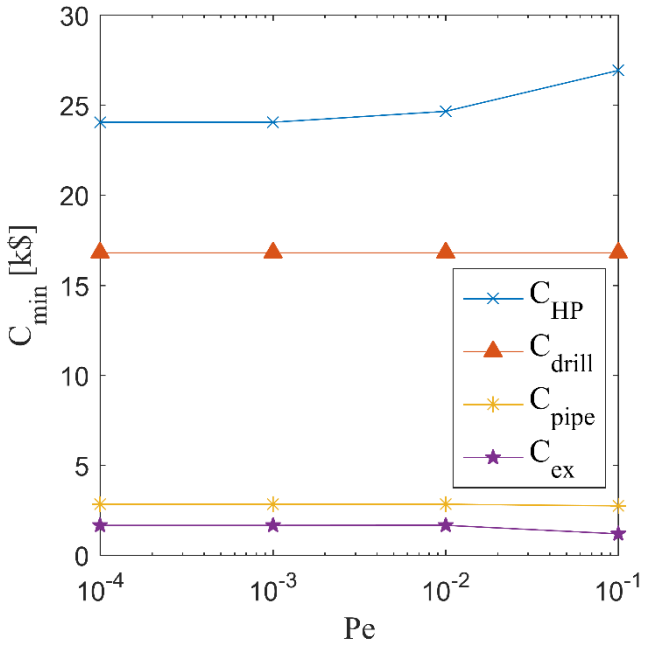

Figure 3.5: Initial cost distribution for the optimized design as a function of Pe for $k_g = 1.5$ W m^{-1} K^{-1}

A detailed analysis of all the initial costs for $k_g = 1.5$ W m^{-1} K^{-1} is presented in Figure 3.5. It can be seen that the drilling cost does not change with Pe since the borefield layout and the borehole depth H do not change in this case as seen in Figure 3.4 and Table 3.3. The piping cost is mostly governed by the value of H and by the number of boreholes, and again, because these values do not change in the scenarios of Figure 3.5, the piping cost is relatively constant. It is only marginally affected by the fact that B is smaller as Pe increases. On the other hand, excavation cost is lower for higher Pe because this cost is significantly affected

by B (see Eq. (3.6)). Heat pump cost is higher at large Pe values since f_{opt} is also higher and this cost is calculated with the maximum heating load which depends on f, see Eqs. (3.4) and (3.18). Note that a similar behavior regarding initial cost was observed for all the k_g values considered in this study.

Table 3.3: Optimal layout of boreholes as a function of Pe and k_g

		Pe			
		10^{-4}	10^{-3}	10^{-2}	10^{-1}
k_g [W m^{-1} K^{-1}]	1.0	1×6	1×6	1×6	1×7
	1.5	1×5	1×5	1×5	1×5
	2.0	1×5	1×5	1×5	1×5
	2.5	1×5	1×5	1×5	1×4
	3.0	1×4	1×4	1×4	1×4
	3.5	1×4	1×4	1×4	1×4
	4.0	1×4	1×4	1×4	1×3

As seen in Table 3.3, the optimal borefield layout changes with Pe and k_g. A higher ground thermal conductivity allows better conductive heat transfer along the boreholes, thus reducing the required number of boreholes to achieve the same result. A higher flow velocity (i.e., a higher Pe) allows better convective heat transfer along the boreholes, also reducing the required number of boreholes.

One can note in Table 3.3 a particular scenario which seems to stand out from the others. The optimal layout for $Pe=10^{-1}$ and $k_g=1.0$ W m^{-1} K^{-1} is 1×7, but with the same conductivity and smaller Pe values, fewer boreholes are chosen by the optimization procedure. This is a different trend compared to other scenarios at higher conductivities for which the optimal number of boreholes is reduced as Pe increases. The optimization results for layouts of 1×5 and 1×6 with $Pe=10^{-1}$ and $k_g=1.0$ W m^{-1} K^{-1} were observed and it was found that the only design variable changing significantly from the results with 1×7 (optimal layout) is f

which is lower as the number of boreholes decreases. With fewer boreholes, the initial cost decreases but the operational cost increases, so the optimization routine tends to lower the fraction of the load assumed by the GCHP system to counterbalance this increase of operational cost. Optimal total costs for 1×5, 1×6 and 1×7 are all within 1% of each other, with 1×5 having the lowest initial cost but the highest operational cost, and 1×7 having the highest initial cost but the lowest operational cost and the overall lowest total cost. Since the goal of the methodology developed here is to find the minimum total project cost, the 1×7 layout has been selected as the optimal, but one could arguably choose other nearly equivalent designs based on specific techno-economic criteria.

3.5.2. Impact of groundwater flow angle

In order to determine the impact of the groundwater flow angle on the energy and economic performance of the GCHP system, a series of optimizations were performed with borefield layouts ranging from 1×1 to 1×9, for 5 values of groundwater flow angle ($\phi = 0^o$, 22.5^o, 45^o, 67.5^o and 90^o), and the same values of Pe as in Section 3.5.1. The thermal conductivity of the ground k_g and the project duration were set to 3 W m^{-1} K^{-1} and 20 years, respectively. The minimized total cost is reported in Figure 3.6 as a function of ϕ and Pe.

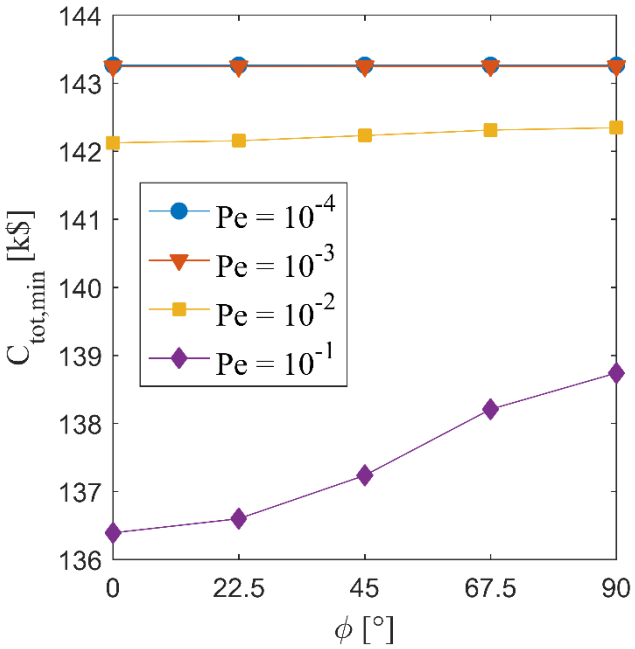

Figure 3.6: Impact of the groundwater flow angle on the project total cost for $k_g = 3$ W·m^{-1} K^{-1} and n = 20 years

As mentioned in Section 3.5.1, the effect of groundwater flow velocity on the total cost of the GCHP system becomes significant only when Pe is greater than 10^{-2}. As a consequence, the flow angle ϕ has a significant impact on the total cost for high values of Pe, as can be seen in Figure 3.6. This figure demonstrates that the heat transfer is enhanced when the groundwater flow axis is perpendicular to the borefield axis (when all boreholes are on the same line). This is represented in the simulations by a flow angle of $\phi = 0^o$. On the contrary, the worst case scenario, i.e., the flow angle at which the total cost assumes its highest value, occurs when the borefield and flow axis coincide, i.e., with a flow angle of $\phi = 90^o$. It is noteworthy to mention that the difference between the best and the worst case scenarios for the total cost when $Pe = 10^{-1}$ is only 2350$, which represents an increase of only 1.7%.

Therefore, although it was shown in Figure 3.6 that the groundwater flow angle influenced the total cost of the system (especially at high values of Pe), the net gain that could be obtained by choosing the optimal orientation appears to be small compared to the order of magnitude of the total cost of the system. This result can appear to be somewhat different

from what previous studies focusing on heat transfer around boreholes in the presence of groundwater flows have concluded [5], [6], [41], i.e., that the orientation of the groundwater flow greatly influences the heat transfer performance and the outlet fluid temperature of the borefield. However, this influence appears to be relatively low on the total cost, as discussed previously.

The small differences detected can be explained by the combined usage of a synthetic load profile and a heat recovery strategy, both discussed in Section 3.3.1. The fraction f is defined with respect to the maximum heating load and is used to shave the load profile, as explained previously. This means that the GCHP system provides a constant amount of heat to the building during a certain period of the year. As a comparison, the fraction of the heating load assumed by the GCHP system in [5] varies for every month of the simulation, and no cooling loads were considered during the summer. In the present chapter, cooling loads are used to regenerate the thermal potential of the ground, thus lowering the impact of groundwater flow. When Pe is small (i.e. $Pe \leq 10^{-3}$), heat conduction is dominant and all the boreholes will benefit from the heat recovery since the groundwater flow will not induce a significant transport of the heat in the ground. When the borefield axis coincides with the flow axis ($\phi = 90^{o}$), and if Pe is high enough to enable heat advection (i.e. $Pe \geq 10^{-2}$), it is possible that only a certain number of boreholes could benefit during the winter from the heat recovery in the summer depending on the flow velocity. This effect is tied to the groundwater flow angle, as the heat recovery will be less and less significant as the angle decreases, i.e., it is maximum when $\phi = 90^{o}$ and minimum when $\phi = 0^{o}$.

Table 3.4: Impact of the flow angle ϕ on the optimal value of the design variables, at $Pe = 10^{-1}$ and $k_g = 3$ W m^{-1} K^{-1}

Variables	Units					
ϕ	[°]	0	22.5	45	67.5	90
$\left(N_x \times N_y\right)_{opt}$	[-]	1×4	1×4	1×4	1×4	1×4
H_{opt}	[m]	105.00	105.00	105.00	105.00	105.00
B_{opt}	[m]	3.83	4.12	5.08	6.70	8.00
f_{opt}	[%]	90.00	90.00	90.00	90.00	90.00

The effect of the flow angle on the optimal design variables is presented in Table 3.4 for $Pe = 10^{-1}$. It can be seen that only the distance between adjacent boreholes B is influenced by the flow angle. This can be explained by considering the thermally affected zone around each borehole, as seen in Figure 3.3. When $\phi = 0^o$, the borefield axis is perpendicular to the flow axis and the boreholes can be close to each other since their zones are mainly downstream. On the contrary, when the borefield axis and the flow axis are aligned, i.e., $\phi = 90^o$, the boreholes must be distant from each other so that their thermal zones do not overlap too much.

3.5.3. Impact of project duration on total cost

A third series of optimizations was completed to study the impact of the project duration on the total cost. Borehole layouts ranging from 1×1 to 1×9 were considered, with 6 values for the project duration, ranging from 5 to 30 years. The same values of Pe as in Section 3.5.1 and 3.5.2 were considered, with a ground thermal conductivity k_g of 3.0 W m^{-1} K^{-1} and a groundwater flow angle $\phi = 0^o$. The results of the optimization are shown in Figure 3.7.

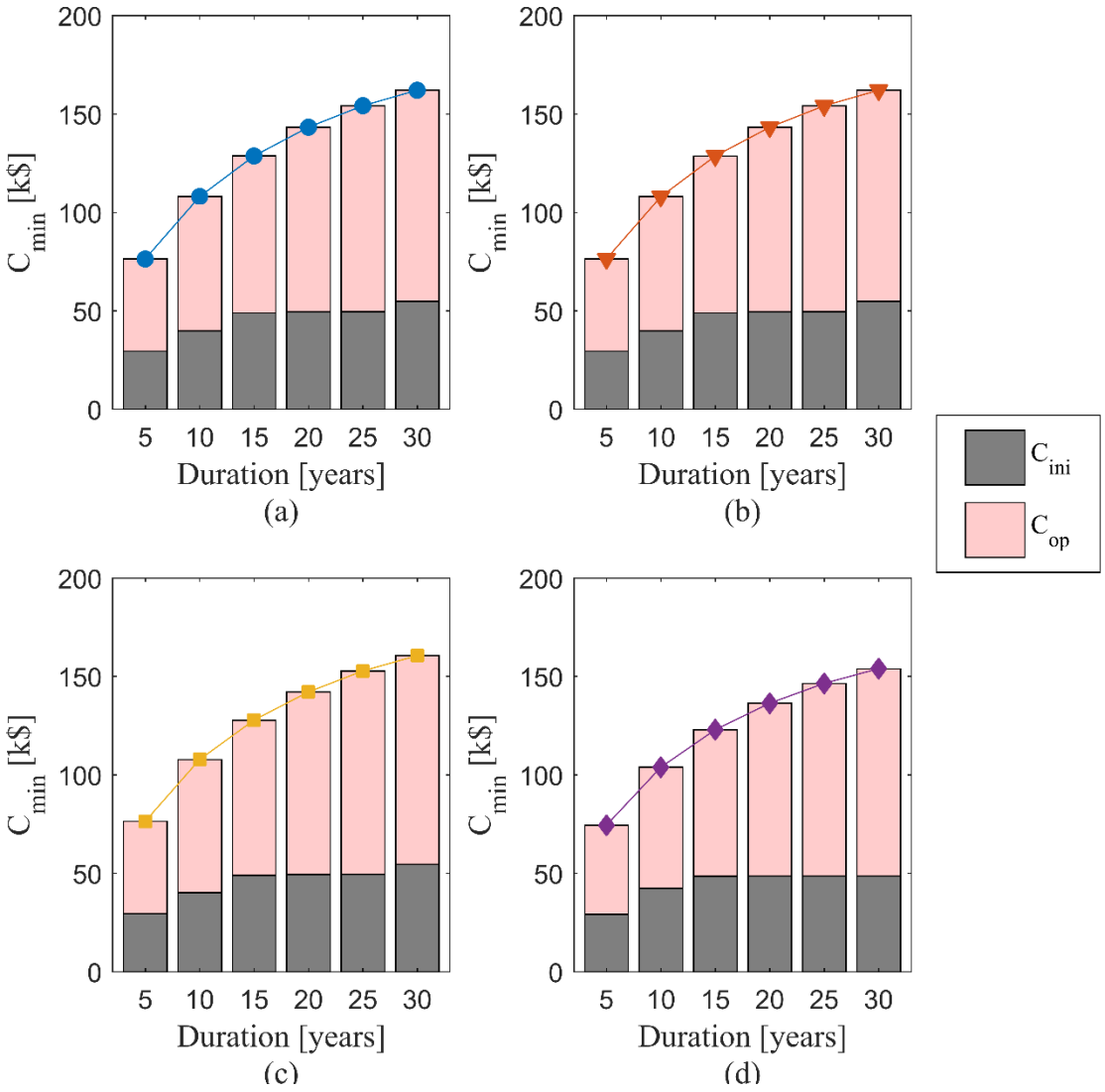

Figure 3.7: Impact of the project duration on minimized costs $(C_{tot} = C_{ini} + C_{op})$ for $k_g = 3$ W m^{-1} K^{-1}: **(a)** $Pe = 10^{-4}$, **(b)** $Pe = 10^{-3}$, **(c)** $Pe = 10^{-2}$, and **(d)** $Pe = 10^{-1}$

As mentioned in the previous sections, the Péclet number only starts to influence the total cost when it reaches relatively high values (i.e., $Pe \sim 10^{-2}$). With the increase of the project duration, the total cost also increases because operational cost must be paid for every added year. However, since every annual money flux is converted into its present value, as shown in Eq. (3.2), the total cost increase is reduced. To better understand this, both the initial and operational costs are also presented in Figure 3.7. It should be noted that in order to simplify

the display of the results, annual operational costs have been summed for every project duration (n):

$$C_{op,n} = \sum_{i=1}^{n} C_{a,i} \left(1+j\right)^{-i} \tag{3.33}$$

It can be seen that for $Pe = 10^{-1}$, the initial cost essentially stops changing at a specific duration, because the optimized layout and variables also stop changing, except for B showing variations of the order of 10%. However, these variations are not large enough to significantly influence the total cost. When the simulation reaches this state, the heat loads in the ground q_g do not vary from year to year, leading to constant annual operational cost $(C_{a,i})$. The total operational cost $(C_{op,n})$ always increases due to the additional years as expected, and the effect of discounting operational costs is easily visible when the optimized design stops changing.

The results presented in this section can also provide insights on the result of individually minimizing the initial and operational costs. From Eq. (3.2), it can be seen that when varying n, the number of years of the project, one actually changes the weight put on operational cost in the calculation of the total cost. In other words, by varying n, it is possible to generate the equivalent of a Pareto front to show the lowest operational cost for a given initial cost, and vice versa. For a given value of n and Pe, the initial cost in Figure 3.7 was reported in Figure 3.8 as a function of the average annual operational cost, calculated as:

$$C_{a,average} = C_{op,n} \left[\frac{j}{\left(1+j\right)^{n} - 1} \right] \tag{3.34}$$

The reported curves correspond to the best designs from a multi-optimization point-of-view. For a given initial cost, the curve reveals the minimum possible operation cost. The zone above the curves in Figure 3.8 corresponds to the accessible design space, whereas the zone below is "inaccessible" (i.e., no possible designs fall within that region). Because the initial cost is essentially constant in a portion of the $Pe = 10^{-1}$ curve, it is possible to obtain a smaller operational cost without increasing the initial cost by using the same GCHP system for a longer duration. Depending on the importance given by the designers to initial vs operation

costs, one could select a point on these figures that will have a lower initial cost but a higher average annual operational cost.

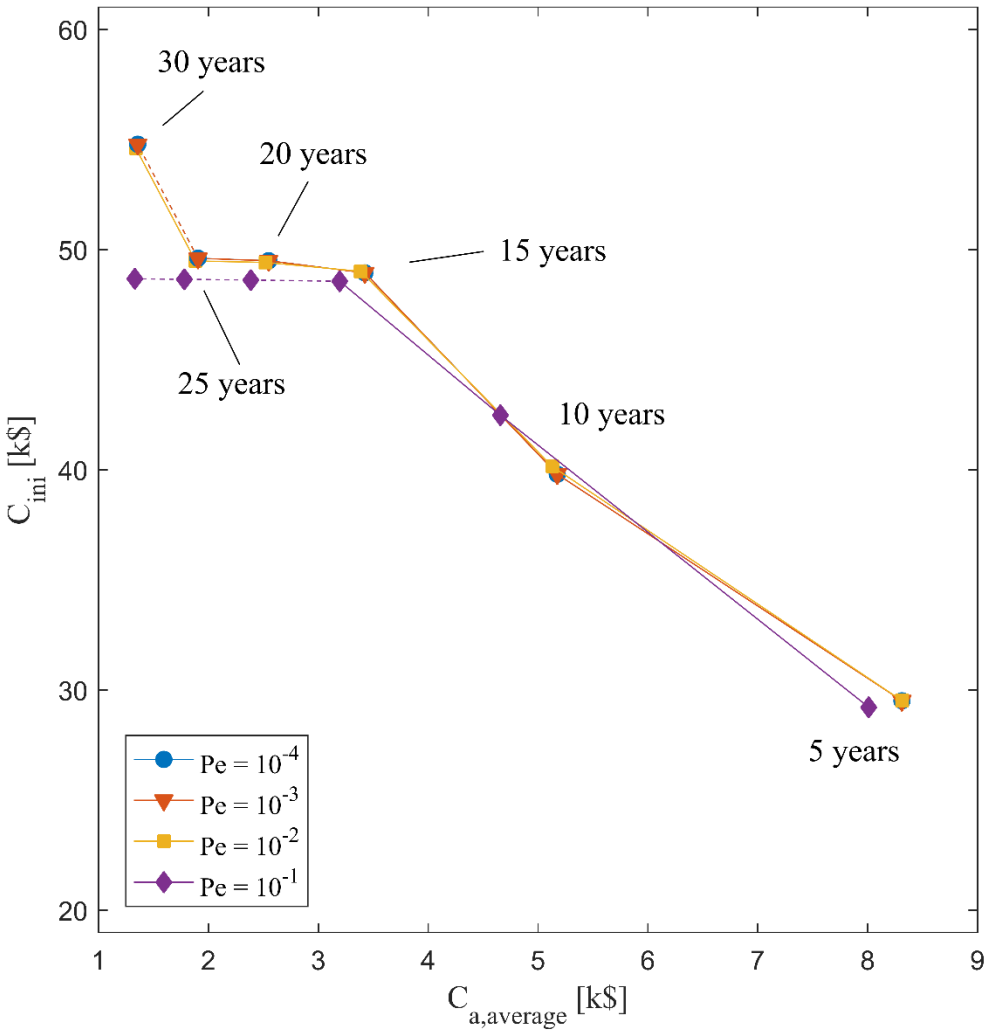

Figure 3.8: Comparison of the minimum initial cost versus minimum operation cost for different Pe values with $k_g = 3\,\mathrm{W\,m^{-1}\,K^{-1}}$ and $\phi = 0^{o}$

3.5.4. Optimized designs under off-design operating conditions

In the methodology described previously, it was assumed that the groundwater flow direction and velocity were known, as well as the ground thermal conductivity. In reality, such

parameters may not always be accurately known or not known at all [42]. In this section, the economic effect of using optimized designs under off-design conditions is analyzed for different flow angles and velocities.

In order to evaluate the largest possible impacts, simulations have been realized with a 1×4 layout for the extreme values of Pe and ϕ tested, i.e., $Pe=10^{-4}$ vs 10^{-1} and $\phi=0^{o}$ vs 90^{o}, with a ground thermal conductivity k_g of 3.0 W m^{-1} K^{-1}, and a project duration of 20 years. First, the optimization routine was run to find the optimal design for each case. Then, a simulation was performed with these optimized designs, but with a flow velocity or angle different than the values used for the optimization. It should be noted that initial costs do not vary between optimal design and off-design simulations, since the same values for H, B and f are used, see Eqs. (3.3)-(3.8). A summary of the results is presented in Table 3.5.

Table 3.5: Effect on the operational cost of operating an optimized design in off-design hydrogeological conditions for $k_g=3$ W m^{-1} K^{-1} and n = 20 years

	Scenario 1		Scenario 2		Scenario 3		Scenario 4	
	Design optimization	Off-design simulation	Design optimization	Off-design simulation	Design optimization	Off-design simulation	Design optimization	Off-design simulation
Pe [-]	10^{-1}	10^{-4}	10^{-4}	10^{-1}	10^{-1}	10^{-1}	10^{-1}	10^{-1}
ϕ [°]	0	0	0	0	0	90	90	0
C_{op} [k$]	87.8	95.7	93.8	87.5	87.8	91.1	88.9	87.5
Difference		+5.8%		–4.4%		+2.4%		–1.0%

Some interesting observations can be made regarding these results. First, the impact of the groundwater flow velocity on the economic performance of the project is greater when a high velocity (i.e., $Pe=10^{-1}$) is assumed but the design is performing in a low velocity geological environment (scenario 1 in Table 3.5), leading to an increase of operation cost of 5.8%. In this case, the GCHP system is designed to rely on the convective heat transfer in the ground,

which is mostly absent with $Pe = 10^{-4}$. On the other hand, if a slow flow is assumed but the design is placed under a high Pe condition (scenario 2), more savings than expected are realized and as a result, the operational cost is reduced by 4.4% compared to the prediction. This is due to the more effective heat transfer along the boreholes induced by the faster flow, as discussed in Section 3.5.2. It can thus be noted that, for the cases considered, the economic consequences on operations under off-design conditions are worst if the groundwater flow velocity is overestimated.

Second, the impact of the groundwater flow angle has been tested for a fixed velocity ($Pe = 10^{-1}$), because previous observations in Section 3.5.2 have shown that the effect of the angle is only visible under high velocity conditions. If a system is designed with $\phi = 0^{o}$, i.e., with the borehole axis perpendicular to the flow axis, but is used under $\phi = 90^{o}$ condition (scenario 3), i.e., with the borehole axis parallel to the flow axis, the operation cost is increased by 2.4%. This is mainly due to the thermal interactions between boreholes (i.e., overlapping of the thermally affected zones around the boreholes), which lowers the overall borefield performance, as discussed in Section 3.5.2. On the other hand, a system designed for $\phi = 90^{o}$ but used with $\phi = 0^{o}$ (scenario 4) allows a 1.0% reduction on the operation cost, since thermal zones will no longer overlap. It can be observed that the impact of the groundwater flow angle on the cost is much lower than the impact of the flow velocity.

3.6. Conclusions

The goal of this chapter was to introduce a new sizing methodology that takes into account groundwater flow. This was achieved by combining G-functions based on analytical models with economic optimization of the total cost of a GCHP project. The procedure included a calculation of the initial costs and of the annual operational costs. A parametric study has been completed to measure the impact of the groundwater flow velocity and angle with respect to the borefield on the economics of a project, as well as the influence of the ground thermal conductivity on the performance of the system.

During the study, it was found that ground thermal conductivity greatly influences the total cost, with high values of k_g leading to more economical systems, but that the groundwater flow impact on total cost only becomes apparent for high velocities, i.e., $Pe \geq 10^{-2}$. The groundwater flow angle was found to be less sensitive, since the net economic gain that could be obtained by choosing the optimal orientation appeared to be small compared to the total cost of the system (i.e., less than 2%). The difference on the borefield outlet temperature caused by a bad flow orientation documented in previous studies was observed, but its influence on the total cost was found to be low.

The equivalent of a Pareto front was plotted to allow a simultaneous comparison of the initial and operational costs. For all Pe values, the higher the initial cost, the lower the operational cost. However, it was found that several optimal designs when $Pe = 10^{-1}$ exhibited very similar initial costs but different operational costs. Such information could be used in a multi-criterion decision-making process. Finally, optimized designs were tested under off-design operating conditions. One could observe that the economic consequences of operations under off-design conditions are far worse if the groundwater flow velocity is overestimated. This could lead to an increase of operational cost of 5.8% if the project is designed with a fast flow velocity, but used under a slow flow velocity, while having the optimal flow angle in both scenarios. A wrong estimation of the flow angle could only lead to an increase of operational cost of 2.4% compared to the best design under the fastest flow velocity.

The sizing methodology introduced here provides a viable design tool for real-life applications. Future work could include the realization of tests for reducing uncertainties on ground thermal conductivity and groundwater flow properties [43]. Although these tests are expensive, they could provide a better understanding of the ground properties, which could lead to better optimization results and lower total costs. Possible freezing of groundwater around the boreholes could also be taken into account [44]. In different geological environments, groundwater may only flow along a portion of the boreholes or its velocity may change along the borehole, hence the necessity to further develop the groundwater flow model [45]. Different building load profiles could also be tested [46]. Finally, simulations for different ranges of k_g, Pe and ϕ could be made to improve the range of validity of this

methodology, in order to produce a user-friendly, practical design tool, such as a spreadsheet or a graphic user interface. Such a tool would be helpful to facilitate the deployment of GCHP systems.

CHAPTER 4 CONCLUSION

The main objective of this work was to develop a new sizing methodology for cost minimization of ground-coupled heat pump systems that takes into account groundwater flow. The sizing procedure included a calculation of the initial and annual operational costs, which is essential for minimization of the project's total cost. Design parameters included hydrogeological data, building thermal loads and GCHP system costs, such as the prices for each piece of equipment, the electricity rates, the ground thermal conductivity, and the groundwater flow properties. In order to improve actual design methodologies, G-functions based on analytical models were included within the economic optimization of the total cost of a GCHP project. Instead of using a correlation for the calculation of G-functions, analytical models were solved for 20 different times, logarithmically spaced across the entire duration of each simulation. Interpolation with spline functions was used to compute the values of the G-functions for every other intermediate time, with an average absolute difference of 0.02% between the interpolated values and those computed with the model. A mathematical simplification for the computation of G-functions during the energy simulation of the GCHP project enabled significant time reduction for the optimization routine, i.e., computation time can be cut by up to 25%. The simplification is a new addition to current methodologies using G-functions.

A parametric study was realized to determine the influence of the ground thermal conductivity and groundwater flow on the economics of a project. It was shown that the ground thermal conductivity greatly influences the project total cost: high values of k_g result in economical systems. Groundwater flow velocity was found to be more influential than the flow angle, particularly when the velocity is overestimated. However, almost no effect on the economics is visible if the flow velocity is relatively low, i.e., if $Pe \lesssim 10^{-2}$.

The equivalent of a Pareto front was plotted to allow a simultaneous comparison of the initial and operational costs for a specific case. One could see that the higher the initial cost, the lower the operational cost, with a portion of the front where it is possible to reduce the operational cost without increasing the initial cost, i.e., the same optimal system is used for a longer duration. This approach could be further explored and generalized in future work in order to establish guidelines for multi-criterion decision-making processes.

Overall, the methodology is simple to use, and allows much control by the user on the design parameters that can be incorporated, thus providing a viable design tool for real-life applications. Future work could include testing of different building loads or transient groundwater flow, for example. The economics of hydrogeological and thermal response tests could be added to the methodology, as a better understanding of the ground properties would lead to better optimization results. However, economic viability between the cost of such tests and the cost savings they could allow should be investigated.

Finally, this study represents a significant advancement in geothermal system simulation research, but it is not yet complete as the subjects discussed here could be extended to other horizons. For example, an experimental validation of the methodology over a long period could provide interesting data on the economics of a GCHP system under various groundwater flow conditions. In addition, the MATLAB program developed for this project requires some expertise from the designer in order to be used correctly in its current form. The development of a graphic user interface would be a more convenient tool for a larger audience.

REFERENCES

[1] I. E. Akpan, M. Sasaki, and N. Endoh, "Optimization of Domestic-Size Renewable Energy System Designs Suitable for Cold Climate Regions," *JSME Int. J. Ser. B Fluids Therm. Eng.*, vol. 49, no. 4, pp. 1241–1252, 2006.

[2] I. Staffell, D. Brett, N. Brandon, and A. Hawkes, "A review of domestic heat pumps," *Energy Environ. Sci.*, vol. 5, no. 11, pp. 9291–9306, Oct. 2012.

[3] R. Fan, Y. Jiang, Y. Yao, D. Shiming, and Z. Ma, "A study on the performance of a geothermal heat exchanger under coupled heat conduction and groundwater advection," *Energy*, vol. 32, no. 11, pp. 2199–2209, Nov. 2007.

[4] S. Bertagnolio, M. Bernier, and M. Kummert, "Comparing vertical ground heat exchanger models," *J. Build. Perform. Simul.*, vol. 5, no. 6, pp. 369–383, Nov. 2012.

[5] J. C. Choi, J. Park, and S. R. Lee, "Numerical evaluation of the effects of groundwater flow on borehole heat exchanger arrays," *Renew. Energy*, vol. 52, pp. 230–240, Apr. 2013.

[6] A. Tolooiyan and P. Hemmingway, "A preliminary study of the effect of groundwater flow on the thermal front created by borehole heat exchangers," *Int. J. Low-Carbon Technol.*, vol. 9, no. 4, pp. 284–295, Dec. 2014.

[7] W. Thomson, "On a Universal Tendency in Nature to the Dissipation of Mechanical Energy," *Proc. R. Soc. Edinb.*, vol. 3, pp. 139–142, Jan. 1857.

[8] J. W. Lund and T. L. Boyd, "Direct utilization of geothermal energy 2015 worldwide review," *Geothermics*, vol. 60, pp. 66–93, Mar. 2016.

[9] M. Younis, T. Bolisetti, and D. S.-K. Ting, "Ground source heat pump systems: current status," *Int. J. Environ. Stud.*, vol. 67, no. 3, pp. 405–415, Jun. 2010.

[10] Hydro-Québec, "Leading the energy revolution," *Hydro-Québec*, 2017. [Online]. Available: http://hydroquebec.com/about/our-energy/. [Accessed: 16-Apr-2017].

[11] A. Mustafa Omer, "Ground-source heat pumps systems and applications," *Renew. Sustain. Energy Rev.*, vol. 12, no. 2, pp. 344–371, Feb. 2008.

[12] H. V. Nguyen, Y. L. E. Law, M. Alavy, P. R. Walsh, W. H. Leong, and S. B. Dworkin, "An analysis of the factors affecting hybrid ground-source heat pump installation potential in North America," *Appl. Energy*, vol. 125, pp. 28–38, Jul. 2014.

[13] P. Eskilson, "Thermal analysis of heat extraction boreholes," *MyScienceWork*, Jan. 1987.

[14] M. G. Sutton, D. W. Nutter, and R. J. Couvillion, "A Ground Resistance for Vertical Bore Heat Exchangers With Groundwater Flow," *J. Energy Resour. Technol.*, vol. 125, no. 3, pp. 183–189, Aug. 2003.

[15] N. Diao, Q. Li, and Z. Fang, "Heat transfer in ground heat exchangers with groundwater advection," *Int. J. Therm. Sci.*, vol. 43, no. 12, pp. 1203–1211, Dec. 2004.

[16] N. Molina-Giraldo, P. Blum, K. Zhu, P. Bayer, and Z. Fang, "A moving finite line source model to simulate borehole heat exchangers with groundwater advection," *Int. J. Therm. Sci.*, vol. 50, no. 12, pp. 2506–2513, Dec. 2011.

[17] A. Angelotti, L. Alberti, I. La Licata, and M. Antelmi, "Energy performance and thermal impact of a Borehole Heat Exchanger in a sandy aquifer: Influence of the groundwater velocity," *Energy Convers. Manag.*, vol. 77, pp. 700–708, Jan. 2014.

[18] A. Angelotti, L. Alberti, I. L. Licata, and M. Antelmi, “Borehole Heat Exchangers: heat transfer simulation in the presence of a groundwater flow,” *J. Phys. Conf. Ser.*, vol. 501, no. 1, p. 012033, 2014.
[19] J. A. Rivera, P. Blum, and P. Bayer, “Analytical simulation of groundwater flow and land surface effects on thermal plumes of borehole heat exchangers,” *Appl. Energy*, vol. 146, pp. 421–433, May 2015.
[20] A. Liuzzo-Scorpo, B. Nordell, and S. Gehlin, “Influence of regional groundwater flow on ground temperature around heat extraction boreholes,” *Geothermics*, vol. 56, pp. 119–127, Jul. 2015.
[21] S. Geng, Y. Li, X. Han, H. Lian, and H. Zhang, “Evaluation of Thermal Anomalies in Multi-Boreholes Field Considering the Effects of Groundwater Flow,” *Sustainability*, vol. 8, no. 6, p. 577, Jun. 2016.
[22] M. Tye-Gingras and L. Gosselin, “Generic ground response functions for ground exchangers in the presence of groundwater flow,” *Renew. Energy*, vol. 72, pp. 354–366, Dec. 2014.
[23] S. Kavanaugh and K. Rafferty, *Ground-Source Heat Pumps : Design of Geothermal Systems for Commercial and Institutional Buildings*. Atlanta : American Society of Heating, Refrigerating and Air-Conditioning Engineers, 1997.
[24] F. Robert and L. Gosselin, “New methodology to design ground coupled heat pump systems based on total cost minimization,” *Appl. Therm. Eng.*, vol. 62, no. 2, pp. 481–491, Jan. 2014.
[25] B. Hénault, P. Pasquier, and M. Kummert, “Financial optimization and design of hybrid ground-coupled heat pump systems,” *Appl. Therm. Eng.*, vol. 93, pp. 72–82, Jan. 2016.
[26] P. Pasquier and D. Marcotte, “Efficient computation of heat flux signals to ensure the reproduction of prescribed temperatures at several interacting heat sources,” *Appl. Therm. Eng.*, vol. 59, no. 1–2, pp. 515–526, Sep. 2013.
[27] Mathworks, “MATLAB Documentation, R2016b,” 2016. [Online]. Available: https://www.mathworks.com/help/.
[28] R. Croteau and L. Gosselin, “Correlations for cost of ground-source heat pumps and for the effect of temperature on their performance,” *Int. J. Energy Res.*, vol. 39, no. 3, pp. 433–438, Mar. 2015.
[29] A. Chiasson and A. O’Connell, “New analytical solution for sizing vertical borehole ground heat exchangers in environments with significant groundwater flow: Parameter estimation from thermal response test data,” *HVACR Res.*, vol. 17, no. 6, pp. 1000–1011, Dec. 2011.
[30] W. Zhang, H. Yang, X. Guo, M. Yu, and Z. Fang, “Investigation on groundwater velocity based on the finite line heat source seepage model,” *Int. J. Heat Mass Transf.*, vol. 99, pp. 391–401, Aug. 2016.
[31] Z. Deng, S. J. Rees, and J. D. Spitler, “A Model for Annual Simulation of Standing Column Well Ground Heat Exchangers,” *HVACR Res.*, vol. 11, no. 4, pp. 637–655, Oct. 2005.
[32] D. Marcotte and P. Pasquier, “Fast fluid and ground temperature computation for geothermal ground-loop heat exchanger systems,” *Geothermics*, vol. 37, no. 6, pp. 651–665, Dec. 2008.
[33] M. Tye-Gingras and L. Gosselin, “Generic ground response functions for ground exchangers in the presence of groundwater flow,” *Renew. Energy*, vol. 72, pp. 354–366, Dec. 2014.

[34] J. Hecht-Méndez, M. de Paly, M. Beck, and P. Bayer, "Optimization of energy extraction for vertical closed-loop geothermal systems considering groundwater flow," *Energy Convers. Manag.*, vol. 66, pp. 1–10, Feb. 2013.
[35] R. Croteau and L. Gosselin, "Correlations for cost of ground-source heat pumps and for the effect of temperature on their performance," *Int. J. Energy Res.*, vol. 39, no. 3, pp. 433–438, Mar. 2015.
[36] Hydro-Québec, "Business | Rates and billing | Rates | Rates for Business Customers | Rate G | Hydro-Québec," 2013. [Online]. Available: http://www.hydroquebec.com/business/rates-and-billing/rates/electricity-rates-business-customers/rate-g/.
[37] Minister of Natural Resources Canada, "Ground-Source Heat Pump Project Analysis Chapter," RETScreen International, 2005.
[38] D. Marcotte, P. Pasquier, F. Sheriff, and M. Bernier, "The importance of axial effects for borehole design of geothermal heat-pump systems," *Renew. Energy*, vol. 35, no. 4, pp. 763–770, Apr. 2010.
[39] L. Lamarche, S. Kajl, and B. Beauchamp, "A review of methods to evaluate borehole thermal resistances in geothermal heat-pump systems," *Geothermics*, vol. 39, no. 2, pp. 187–200, Jun. 2010.
[40] A. M. MacDonald, L. J. Brewerton, and D. J. Allen, "Evidence for rapid groundwater flow and karst-type behaviour in the Chalk of southern England," *Geol. Soc. Lond. Spec. Publ.*, vol. 130, no. 1, pp. 95–106, Jan. 1998.
[41] H. Wang, C. Qi, H. Du, and J. Gu, "Thermal performance of borehole heat exchanger under groundwater flow: A case study from Baoding," *Energy Build.*, vol. 41, no. 12, pp. 1368–1373, Dec. 2009.
[42] J. Rouleau, L. Gosselin, and J. Raymond, "New concept of combined hydro-thermal response tests (H/TRTS) for ground heat exchangers," *Geothermics*, vol. 62, pp. 103–114, Jul. 2016.
[43] J. Rouleau and L. Gosselin, "Inverse heat transfer applied to a hydrogeological and thermal response test for geothermal applications," *Int. J. Therm. Sci.*, vol. 109, pp. 70–80, Nov. 2016.
[44] T. Zheng *et al.*, "Efficiency and economic analysis of utilizing latent heat from groundwater freezing in the context of borehole heat exchanger coupled ground source heat pump systems," *Appl. Therm. Eng.*, vol. 105, pp. 314–326, Jul. 2016.
[45] X.-R. Kong, Y. Deng, L. Li, W.-S. Gong, and S.-J. Cao, "Experimental and numerical study on the thermal performance of ground source heat pump with a set of designed buried pipes," *Appl. Therm. Eng.*, vol. 114, pp. 110–117, Mar. 2017.
[46] P. Hein, O. Kolditz, U.-J. Görke, A. Bucher, and H. Shao, "A numerical study on the sustainability and efficiency of borehole heat exchanger coupled ground source heat pump systems," *Appl. Therm. Eng.*, vol. 100, pp. 421–433, May 2016.